A Systematic Investigation of Quantum Confinement Effects in Bismuth Nanowire Arrays

Author: James R. Riley

A Systematic Investigation of Quantum Confinement Effects in Bismuth Nanowire Arrays

James Riley

Honors Thesis

Physics Department / Honors Program

College of Arts and Sciences

Boston College

May 8, 2009

Acknowledgements

It is difficult to adequately express my thanks to my adviser, Professor Michael J. Graf. Over the past three years his unique combination of pressure and patience has helped me to become a stronger student and a better researcher. This thesis project wouldn't have been possible without his knowledge, guidance, and insight. I truly appreciate all he has done for me during the course of my college years.

I would like to thank Professor Tito E. Huber for teaching me the pressure injection technique. This method was both highly interesting to learn and vital for the continuation of my research. His generosity in accommodating me at Howard University resulted in a productive and enjoyable experience.

Ryan Johnson was also an immense help during the course of my project. He took a lead role in the series of magnetization experiments and was the first author of the paper that resulted from that research. I owe a debt of gratitude to him for the work he did improving the production of the Au-Ge alloy thin film thermometers; without his study it would have been far more difficult to create a thermometer with low heat capacity. Further, the photolithography instruction and general clean room assistance he provided was invaluable.

Additionally, I am grateful to Professor David Broido , Dr. J.I. Oh, Stephen Shepard, and Karen Chen. Professor Broido provided useful information and conversation regarding 1-D phonon confinement, Dr. Oh instructed me in the use of the L-Edit software, Stephen Shepard taught me several sample fabrication techniques, and Karen Chen assisted me with the assembly of the calorimeter system.

Finally, I would like to thank the Boston College Honors Program for providing me with such an amazing opportunity. Conducting this thesis project was one of the most fulfilling endeavors of my undergraduate career.

Abstract

Bismuth is an interesting element to study because the low effective mass of its charge carriers makes the material sensitive to quantum confinement effects. When bismuth is reduced to the nanoscale two interesting phenomena may occur: it may transition from a semimetal to a semiconductor, or charge carriers in special surface states may begin to dominate the behavior of the material. Arrays of bismuth nanowires of various diameters were studied to investigate these possibilities. The magnetoresistance of the arrays was measured and the period of Shubnikov-de Haas oscillations suggested an increase in the effective mass and density of the material's charge carriers for small nanowire diameters. These increases suggested that electrons were present in surface states and strongly influenced the material's behavior when its dimensions were sufficiently reduced. The magnetization of the nanowire arrays was also measured and the lack of de Haas-van Alphen oscillations for certain diameter nanowires suggested that electrons were not present in surface states and that instead the material was transitioning from a semimetal to a semiconductor. Heat capacity measurements were planned to reconcile the two experiments. My detailed calculations demonstrated that heat capacity measurements were feasible to determine the presence, or absence, of surface charge carriers. Because the electronic contribution to the material's heat capacity is small a calorimeter platform was constructed with ultra-low heat capacity components.

TABLE OF CONTENTS

Introduction

Two important scientific frontiers currently exist: the exploration of very large distances and very small distances. Astrophysics deals with objects millions of light years away from our planet while condensed matter nanophysics deals with atoms and particles at nanometer scale distances. While the prefix “nano” has begun to enter the vocabulary of the American public, many don’t comprehend the fantastically small size of the realm of nanoscale structures.

“Nano” typically describes an object whose dimensions range from 1 to 100 nanometers. One nanometer is one billion times smaller than one meter (1 nm = 10^{-9} m); to put this size scale into perspective, individual atoms, the building blocks of matter, typically have radii only about ten times smaller than one nanometer.

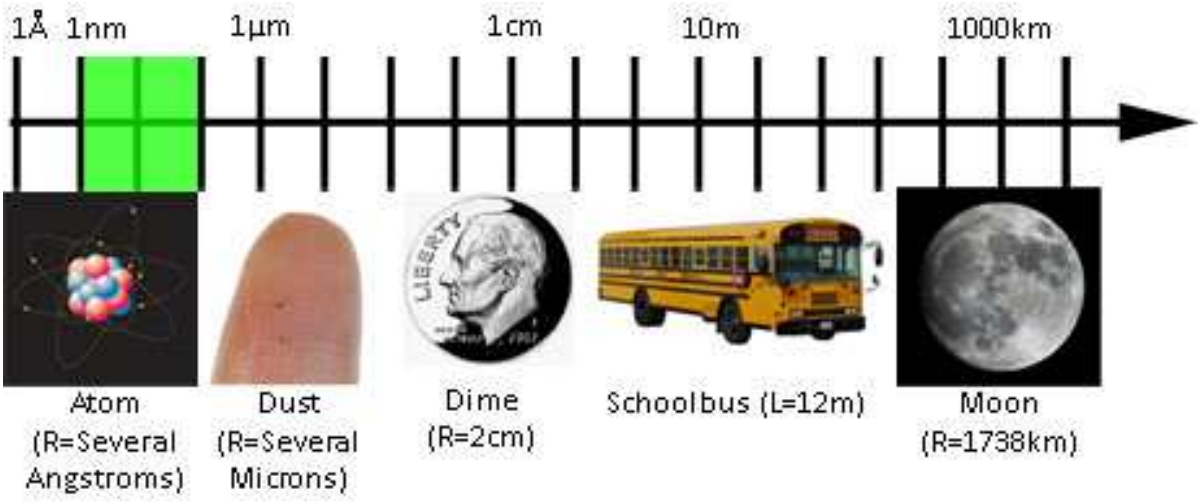

Figure 1: The above images are displayed at their appropriate size scales on a logarithmic plot, in which each step indicates a tenfold increase in size. The square highlighted in green indicates the "nanoscale" region of 1-100 nm.

Scientists are not only interested in studying nanoscale objects because these objects are merely small, however. When lengths are reduced to the nearly atomic level interesting phenomena begin to occur. These phenomena can be described by the laws of quantum physics and are often

contradictory to common sense and human physical intuition. Physicist Richard Feynman even once went as far as to claim that "I think I can safely say that nobody understands quantum mechanics."[1] At the scale that humans are used to (distances measured in cm, m, and km, and masses measured in g and kg) quantum mechanical phenomena are rarely observed. Materials at these larger size scales are usually referred to as existing in the "bulk" state. At smaller size scales, however, particles can exhibit behavior as strange as being present in two different places at once or being instantaneously "aware" of events occurring very far away.[1]

The related fields of nanoscience and nanotechnology emerged to investigate the manner in which the physical laws of the universe are manifested at nearly atomic sizes. There is significant overlap and synergy between these two fields. People who study nanoscience are concerned with the fundamental nature of small objects while those that pursue nanotechnology tend to focus on the unique applications and practical uses of nanoscale materials that result from certain quantum mechanical effects.

One of the hierarchical structures studied by nanoscientists is the nanowire. Nanowires have diameters ranging from one to several hundred nanometers and are typically several microns in length. These parameters describe a structure that is nearly one dimensional in nature. Nanowires are approximately one thousand times thinner than the average human hair.

In this thesis I will describe the systematic investigation of arrays of bismuth nanowires. An array may contain ten billion parallel wires which are uniform in size, are all oriented vertically, and are isolated from one another. A series of research projects was planned to explore the electronic properties of these nanowire arrays. First, magnetoresistance measurements were performed in order to determine how the electrical resistivity of the material responded to an applied magnetic field. Oscillations in the resistivity of certain nanowire arrays demonstrated an increase in the density and

mass of the material's charge carriers from the expected bulk value. This increase suggested that electrons were inhabiting special states on the surfaces of the nanowires. While these states did not significantly affect the bulk material, when the material was reduced to nanowires with small diameters and consequently high surface area to volume ratios, it was possible that the electrons in the surface states were dominating the material's behavior. To further probe this phenomenon I conducted a series experiments to explore how the material magnetized in an applied magnetic field. The analysis of the oscillations (and lack of oscillations) in the magnetization of certain nanowire arrays did not show the enhancement of the charge carrier concentration suggested by the magnetoresistance measurements. In order to reconcile the results of these experiments, I planned a series of measurements of the material's heat capacity. Because the heat capacity of a material is closely related to the behavior of its electrons, the heat capacity measurements were designed to determine whether or not electrons were existing in the special surface states. Because of the extreme difficulty of measuring thermal effects of electrons in such low mass samples, many estimations and calculations were required to create an experimental system. I showed that such a measurement is feasible and I constructed the "first generation" calorimeter platform to carry out the measurement.

Background

Bismuth (Bi) is a highly interesting element to study when it is reduced to the nanoscale. The study of arrays of Bi nanowires is an effective way to explore the variety of electronic properties that make Bi so unique.

There are several characteristic electronic materials: insulators, conductors, semiconductors, and semimetals. It is necessary to use the "band structure model" to describe the differences between these materials. In this model the electrical properties of the material are described by various energy

bands which contain electrons and are separated by forbidden regions or “gaps” in which no electron orbitals exist. The “valence band” of a material is defined as the band of highest energy which is fully occupied by electrons at absolute zero. The next higher energy band is known as the “conduction band.”[2] Electronic conduction is defined as the movement of electrons in the conduction band. Put simply, if the conduction band is partially filled electrons are able to flow because there are empty states to which electrons can move. In full bands there are no empty states for the electrons and so they are unable to move. The energy gap separates these electrons from those in higher energy states. When an electron moves to a empty state it leaves behind a vacant orbital or “hole.” As electrons flow in one direction these holes move in the opposite direction. Because electrons have negative charge holes act as particles with positive charge.

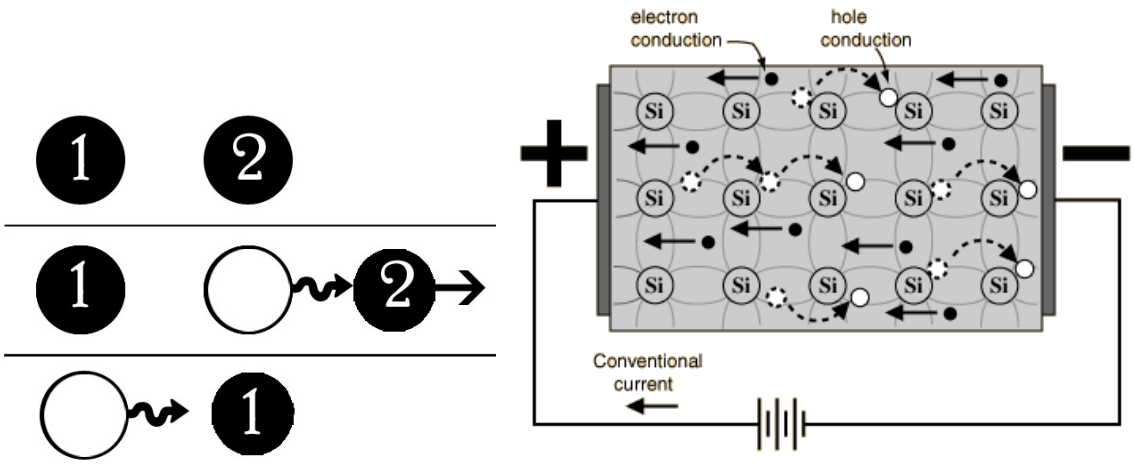

Figure 2: (Left) The diagram demonstrates the apparent movement of holes. The numbered black circles represent two different electrons and the open circle represents a hole. As electrons flow to the right, the hole moves to the left. (Right) Carrier movement in silicon, an actual semiconductor. Electrons flow opposite to what is conventionally considered positive current.[3]

Insulators have full valence bands and an empty conduction bands with a large gaps separating the two and preventing charge carriers (electrons and holes) from moving from one band to the other.[4] Because the conduction band is always empty and the valence band full, electric current cannot flow in

insulators. A second type of material is a metal. Unlike insulators, metals readily allow the flow of electric current. In a metal the carriers partially fill the conduction band. It does not require significant additional energy for electrons to move within a particular band, so little energy is required to promote electrons from filled orbitals to unfilled orbitals. The electrons thus easily move and electrical conduction occurs.[5] The resistivity (current flows more easily through materials with low resistivity values) of a good insulator may be as large as 10^{22} ohm-cm while a metal can have a resistivity as low as 10^{-10} ohm-cm at 1K.[2]

Semiconductors have band structure somewhere between that of insulators and that of metals. They have small band gaps and are insulators at absolute zero but can become conductors when electric fields are applied. Further, carriers can either be thermally excited from the valence to the conduction band, or the material can be doped with an impurity element to increase the number of free charge carriers.[2,4] If the impurity has five valence electrons (phosphorus, for example), in a valence-four semiconductor, the impurity will "donate" one of its electrons. In this case, the number of free electrons will be increased and the semiconductor is referred to as "n-type." If the impurity has three valence electrons (boron, for example), it will be an electron "acceptor" and an abundance of holes will be created. This second type of doping is referred to as "p-type." Further, Because of the ability of semiconducting materials, such as Silicon (Si), to change between conducting and non-conducting states they are commonly used to create transistors—the devices that, by switching on and off, form the foundation of modern computing. Finally, a fourth type of material is a semimetal. Semimetals have offset bands with the conduction band edge having a slightly lower energy than the upper edge of the valence band.[2] The overlap causes a small concentration of holes in the valence band and electrons in the conduction band. This phenomenon occurs because electrons in the valence band can "leak" into the conduction band leaving behind empty states through the process of "tunneling." Tunneling is a quantum mechanical phenomenon which allows particles to cross through seemingly forbidden

regions.[1] Because semimetals have a small number of carriers, semimetals tend to have lower thermal and electrical conductivity values. Many of the interesting properties of Bi are due to the fact that it is a semimetal.

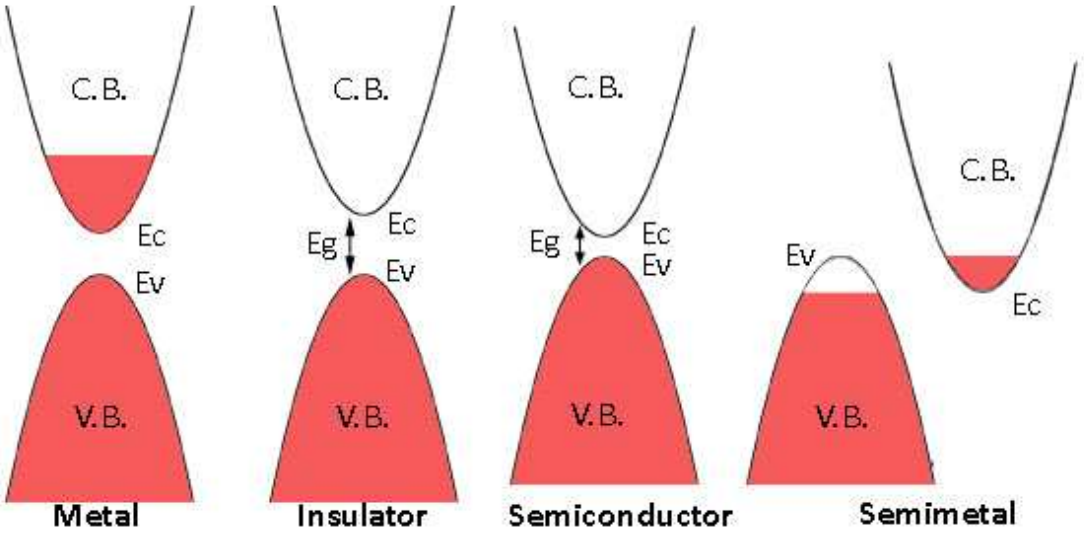

Figure 3: The band structures for four types of materials are shown. The conduction band and valance band are labeled as C.B. and V.B. The conduction band edge energy, the valence band edge energy, and the energy gap are labeled Ec, Ev, and Eg, respectively. The red shading indicates electron occupation and the white indicates vacant orbitals (holes).

One particularly interesting semimetal property of bulk Bi is that the material's electrons have small "effective mass."[6] Within a given material electrons will respond to electric fields as if they have a certain mass. Depending on the material, this mass may differ from the typical mass of a free electron. The effective mass is denoted by the symbol m*.[2] When describing a material's electronic behavior it is necessary to know the effective mass of the carriers as well as the carrier density within the material. For bulk Bi the low temperature effective mass of electrons is equal to the effective mass of holes and has been shown to be $0.065m_e$ where m_e is the rest mass of the free electron.[6,7] Further, the carrier density for both electrons and holes is $3x10^{17}$ cm^{-3} at 2 K, which is much lower (by several orders of magnitude) than the carrier density for typical metals.[8]

When the dimensions of a material are reduced to near the atomic scale the bulk properties listed previously may be altered through the process of "confinement." The small effective masses of the carriers in Bi cause the material to be particularly sensitive to confinement effects. One confinement effect which may occur in Bi is the semimetal to semiconductor (SM-SC) transition. A standard Quantum Mechanics thought experiment is the "infinite potential well," which is also known as the "particle in a box" model. In this situation a region ($0 \leq X \leq L$) of zero potential is bounded by two infinite potential barriers. An electron in this potential well will only be able to exist at discrete quantized energy levels. These energy levels are directly related to the length of the region of zero potential; if the length of the region decreases the gaps between the energy levels will increase.[1]

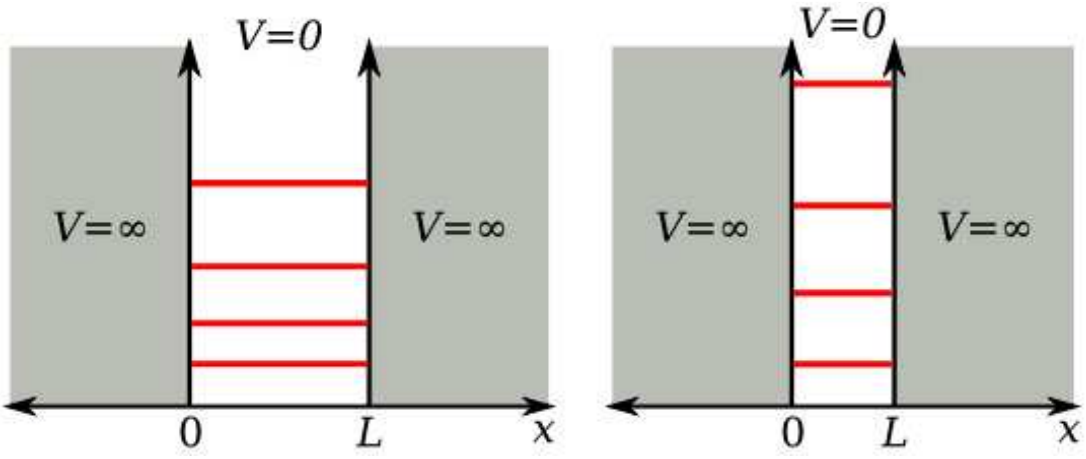

Figure 4: In the infinite potential well a region ($0 \leq X \leq L$) of zero potential (V=0) is bounded by regions of infinite potential. Electrons can only inhabit the quantized energy levels marked in red. If the length of the region of zero potential is reduced the energy levels will become farther apart.[9]

When a material is reduced from a bulk size to a nanoscale size the region which electrons can inhabit decreases. By confining electrons in this way a similar effect to that which occurs in the infinite potential well is produced. In bulk Bi the effective band overlap energy, E_0, and the Fermi energy, E_f, are 37 and 26 meV respectively.[6] If Bi is reduced to a nanowire structure, however, confinement effects that cause E_0 to decrease become relevant at a certain diameter d:

$$d \sim \frac{2\hbar}{\sqrt{2m^* E_0}}$$ [6]

As E_0 decreases the valence and conduction bands of Bi shift apart and the material transitions from a semimetal to a semiconductor. Calculations show that for trigonally oriented nanowires the SM-SC transition occurs around $d \approx 55$ nm.[10]

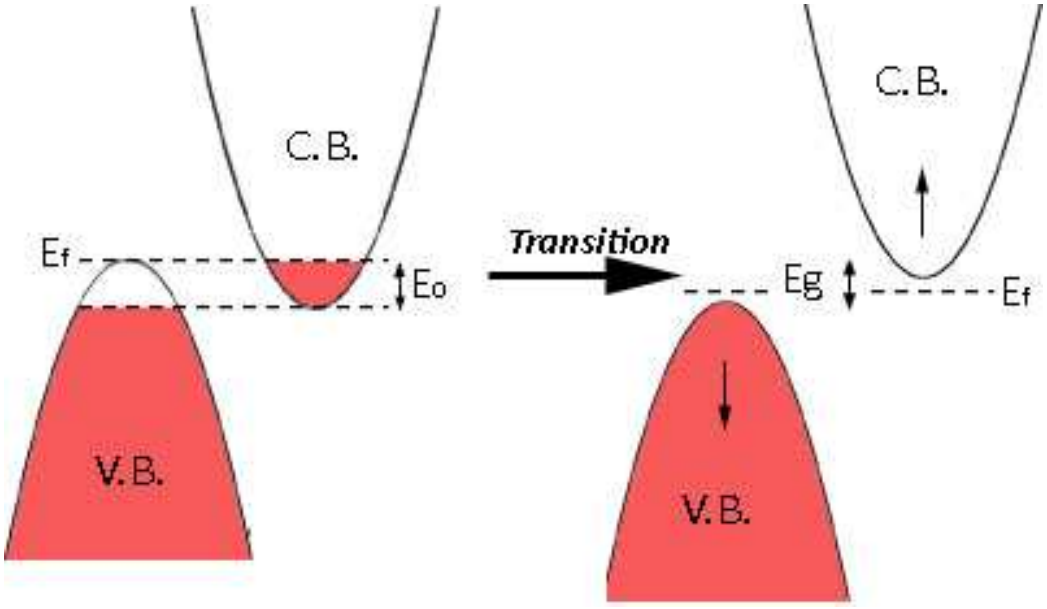

Figure 5: The SM-SC transition occurs when Bi's bands shift so that the energy of the conduction band edge is no longer lower than the valence band edge energy. The material thus gains a small band gap and behaves like a semiconductor. The band overlap energy and the Fermi energy are labeled E_0 and E_F, respectively.

Another intriguing effect that may occur in Bi when its dimensions are confined is the increased significance of "surface states." The boundaries of Bi structures might have layers of more massive electrons in these surface states that could be formed by the spin-orbit interaction that occurs in the presence of the surface electric field.[15] In bulk Bi electrons in surface states would not play a significant role in the behavior of the material because there would be far more electrons existing in conventional states in the volume of the material. However, geometrically, Bi nanowires have very high surface area

to volume ratios and so in nanoscale systems the more massive electrons in surface states could dominate the material's electronic and thermal behavior.[15]

Sample Fabrication

Due to their small size and mass, it would be difficult to obtain electrical and thermal measurements of individual Bi nanowires. Further, single Bi nanowires would have little significance to thermoelectric technology—one of the main potential applications of the structures. An effective way of solving both of these problems is to study arrays of Bi nanowires. Arrays are composed of ten billion (or more) Bi nanowires per mm^2 which all have uniform radius and length.[6] The nanowires would have nm scale diameters, micrometer (1 µm = 10^{-6} m) scale lengths, and would all be oriented in the same direction. Each nanowire is isolated within a template material and does not make electrical contact with any of the other wires.

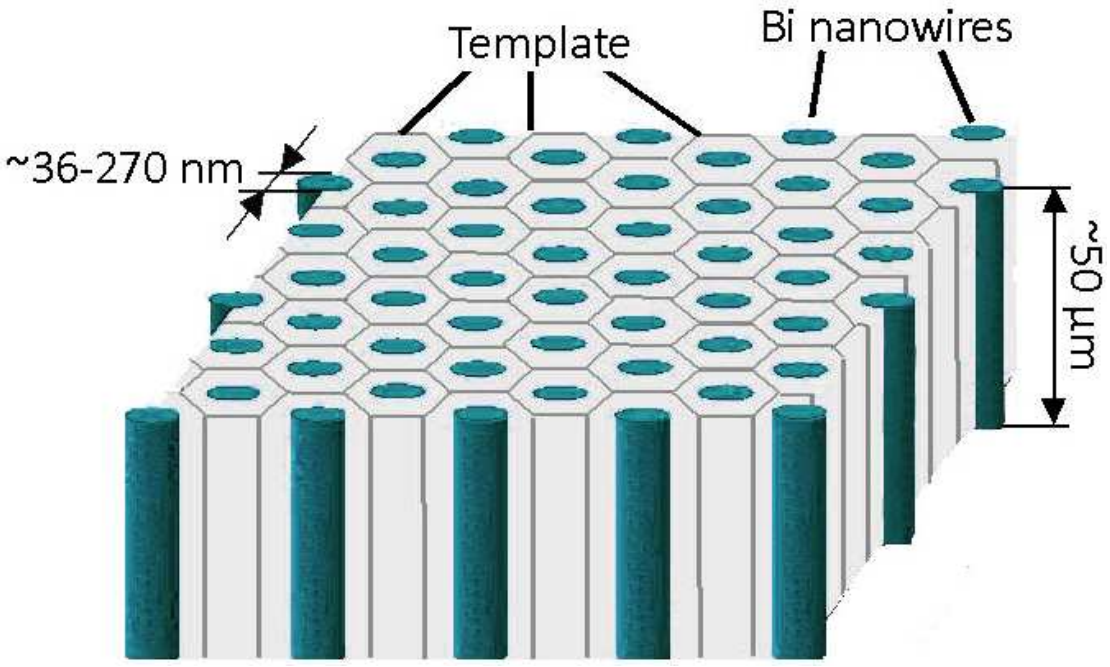

Figure 6: A schematic of a nanowire array. The Bi nanowires are shown in blue and the template material is shown in gray.[12]

Because the nanowires are delicate and small structures the fabrication of an array of uniform nanowires posed a unique challenge.

Professor Tito Huber of Howard University has developed a procedure to consistently produce such arrays. Several nanowire arrays had been prepared previously and were used for the experiments discussed in the **Magnetoresistance Measurement** and **Magnetization Measurement** chapters of this thesis. These arrays, however, had low Bi mass. To measure heat capacity samples with higher amounts of Bi were required. I traveled to Howard University to learn the sample fabrication technique from Professor Huber and to prepare higher Bi mass nanowire array samples.

The first step of the process was the preparation of porous host templates. "Anopore" Porous Anodized Aluminum Oxide (PAAO) templates were used for all the experiments that will be discussed. The Anopore templates were 25 mm in diameter and are 55 micrometers thick. They are produced commercially by Whatman Laboratory Division in Clifton, New Jersey.[11,13] The PAAO templates have nanochannels which are formed via an anodization process.[13] Anodization functions by using an aluminum surface as a positive electrode (anode) and passing a current through an electrolyte solution. Hydrogen is released at the cathode and oxygen at the anode, thus creating a surface of aluminum oxide on the aluminum. The process is performed in an acid solution (usually a dilute polyprotic acid in which the aluminum oxide is only slightly soluble) which balances the oxidation rate and chemically dissolves the aluminum to create a series of hexagonal nanochannels.[14] The anodization process produces an insulator with an array of parallel channels which are mostly not interconnected and are perpendicular to the template surface.[13] The nanochannel diameters are highly uniform. It has been reported that for 32 nm diameter channels the deviation in channel diameter is ± 4 nm.[13] Further, various samples of

nanowire arrays fabricated using the PAAO templates have been measured to have the following diameters with associated errors: 36 ± 3 nm, 60 ± 14 nm, 270 ± 40 nm.[8]

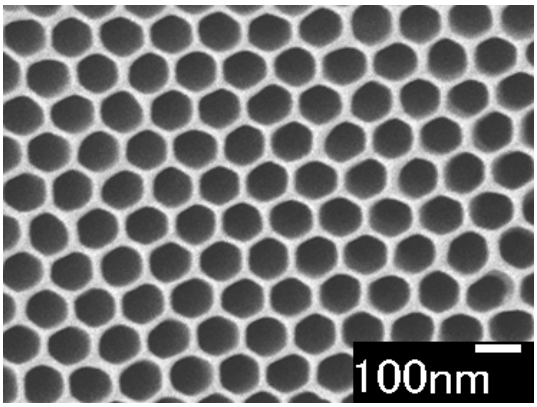

Figure 7: Scanning Electron Microscope (SEM) image of the top view of an empty PAAO template[15]

Once these templates are prepared, they must be filled with Bi. I broke several templates into smaller pieces several mm in size and lashed them together with tungsten wire to form a "stack" of templates. Pieces of mica were placed on either end of the stack. I then positioned the stack inside a quartz tube which was heated and constricted so that it had two chambers connected by a small gap. The stack resided in the lower chamber and I placed solid Bi needles in placed in the upper chamber. The pieces of Bi were 99.999% pure. They were stored in oxygen and were likely oxidized, but the oxide layer or other impurities that may have be present (trace amounts of Iron (Fe) or Copper (Cu)) were removed as "scum" during the course of the procedure.

Next, I placed the filled quartz tube in a furnace and heated it to approximately 300°C to melt the solid Bi. A reactor was used to pressure-inject the liquid Bi down from the upper to the lower chamber and into the PAAO templates. The reactor was home-built and assembled from commercial parts manufactured by Autoclave Engineers. Pressure injection was necessary because Bi does not naturally "wet" insulating materials at its melting point temperature.[13] This means that the liquid Bi will

not naturally flow into the nanochannels of the template. Huber *et al* states that the equation describing the pressure required to inject a non-wetting liquid into a porous material is

$$P = {}^{12}/_{d}$$

where P is pressure measured in kilobars (kbar) and d is the pore diameter measured in nm.[13] Therefore, a modest pressure of 4kbar can be used to inject liquid into any pores with diameters larger than 3 nm. A pressure of approximately 1 kbar was used to fill the template with 270 nm diameter nanochannels. After the liquid Bi was injected, the system was cooled so that the Bi solidified in the template. The pieces of mica on either end of the stack of templates helped to promote directional crystallization of the solid Bi.

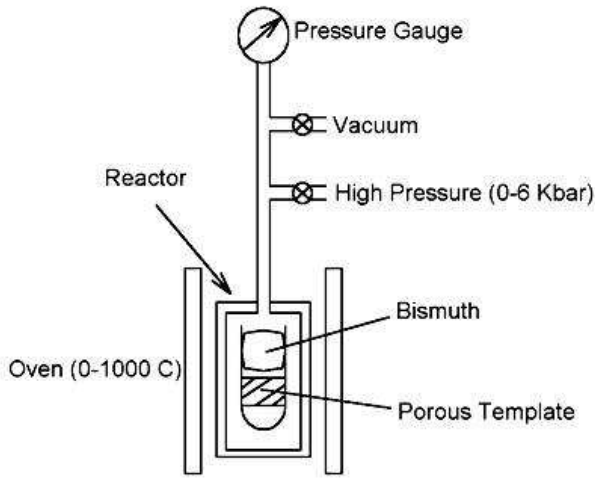

Figure 8: Schematic of the pressure injection system[15]

After I injected the Bi, it was necessary to polish the templates to remove any excess bulk Bi. I did the polishing by hand using a metal polishing disc and sandpapers of various grades of coarseness. It was important not to over-polish the samples. Once the edges of the nanowire arrays were visible I had to take incredible care because the arrays were very fragile and could easily break. Once the bulk Bi was

removed from the edges of the arrays, I could have used a razor blade to extricate individual arrays from the stack. However, because in this case high sample mass was desired, the arrays were left in "stack" form. Two 270 nm diameter nanowire array stacks were prepared, each consisted of 7 arrays and were approximately 360 μm thick.

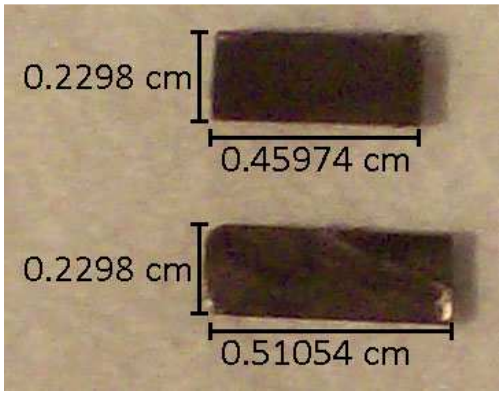

Figure 9: The two nanowire array stacks are depicted above with dimensions indicated.

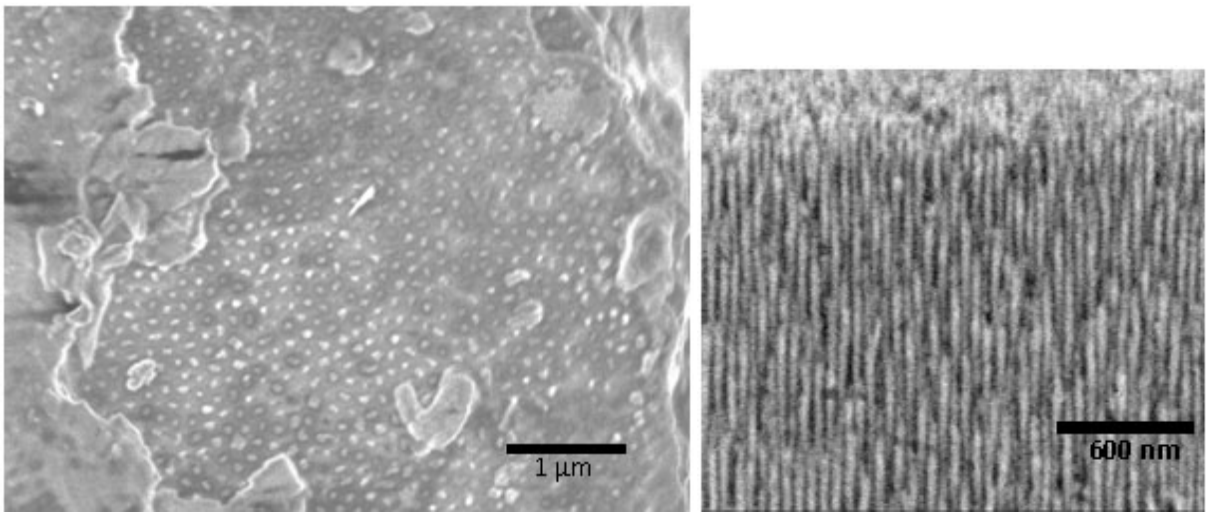

Figure 10: (Left) Top view and (Right) side view of filled nanowire arrays. Both images were taken using a SEM and scale bars are included.[15]

The individual nanowires in the arrays prepared using the pressure injection method are composed of highly oriented crystalline grains.[6] X-Ray Diffraction (XRD) was previously used to

characterize the nanowire arrays.[6] XRD operates by observing how x-rays scatter off atoms and is a powerful analysis technique that can provide detailed structural information about crystalline structures.[14] According to the XRD measurements, more than 90% of the nanowires in the arrays were oriented along the trigonal axis.[6]

Magnetoresistance Measurement

The observation and analysis of magneto-oscillatory effects, such as the de Haas-van Alphen (dHvA) and Shubnikov-de Haas (SdH) effects, was used to probe the nature of the SM-SC transition and to explore the possible existence of surface states. In order to discuss these oscillations it is first important to understand the concept of "Landau levels." If a charged particle is given some initial momentum and subjected to a magnetic field oriented perpendicularly to the particle's direction of motion the particle will begin to move in a circular orbit.

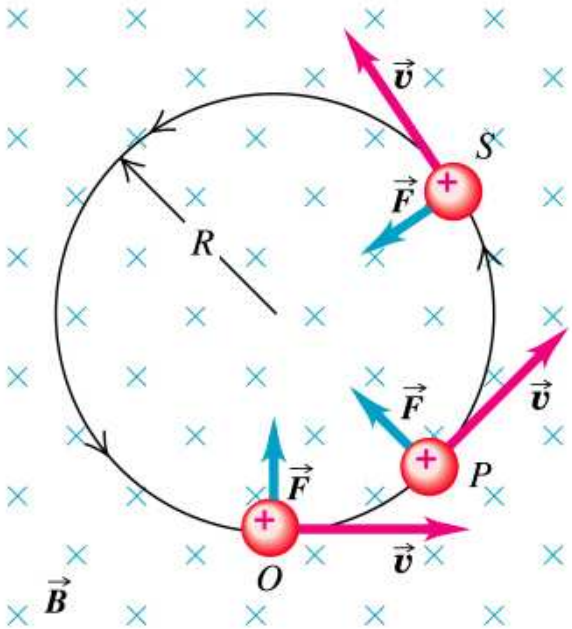

Figure 11: A positive particle is shown and subjected to a magnetic field pointing away from the reader.[16]

The circle, known as the "cyclotron orbit," will have a radius that directly depends on the particle's momentum and on the strength of the magnetic field. As the magnetic field decreases toward zero the cyclotron orbit will tend to increase toward infinity. In the classical physics paradigm an infinite number of cyclotron orbit radii can be realized by continuously varying the particle velocity or the strength of magnetic field. Quantum mechanical laws, however, dictate that only a certain number of discrete quantized orbitals can be achieved. Within a material, Landau levels describe the number of free electron orbitals that coalesce in a single quantized level when a magnetic field is applied.[2]

The quantization of Landau levels leads to a particular phenomenon that can occur when a material is magnetized. For a system of electrons at absolute zero the system's Landau levels are occupied up to a certain level. Only a certain number of electrons can exist in a given level at the same time, and so orbitals at the next highest level will be filled if needed to accommodate extra electrons. The Fermi level will lie in the highest Landau level, even if it is not fully filled. As the applied magnetic field is increased the electrons in the higher partially filled level move down to lower levels because the degeneracy of the electrons increases as the applied field is increased. When no electrons inhabit the higher level, the Fermi level immediately lowers to the level of the highest filled levels.[2] This shift of the Fermi level causes two measureable effects to occur. The dHvA effect describes the oscillation of the magnetic moment of the material and the SdH effect describes the oscillation of the material's conductivity. Both phenomena manifest oscillations which are periodic with the period inversely proportional to the applied magnetic field strength.[2,17]

In order to explore the SdH effect the longitudinal magnetoresistance (LMR) and transverse magnetoresistance (TMR) of arrays of Bi nanowires were measured by Huber *et al* in 2004.[6] For LMR and TMR an applied magnetic field is oriented parallel and perpendicular, respectively, to the current

flowing through the sample being measured. Two-probe measurements were performed by attaching Cu electrodes to the Bi nanowire arrays using silver epoxy contacts.[6] Quasifour-probe measurements were performed on samples in which arrays possessed a thin cap (approximately 0.2 mm) of bulk Bi on either side to promote contact.[6] Zero-field resistance and magnetoresistance measurements were made in two different laboratories. The first was at Boston College which possessed a superconducting magnet and a ^{3}He fridge which could operate from 0 to 9 T and from 1.8 to 300 K, respectively. The second lab was the International Laboratory of High Magnetic Fields and Low Temperatures in Wroclaw, Poland, which operated a 0 to 14 T magnet in the temperature range from 1.8 to 300 K.[6] Arrays of 30, 80, 200, and 270 nm diameter nanowires were studied.[15]

When the 80, 200, and 270 nm diameter nanowire arrays were studied all exhibited SdH oscillations. These oscillations were periodic and could be described by the following equation

$$\Delta\left(\frac{1}{H}\right) = \frac{2\pi}{hc}\frac{1}{A_e}$$

where H is the applied magnetic field and A_e is the extremal cross-sectional area of the Fermi surface perpendicular to the magnetic field.[15] The Fermi surface of a material is an abstract 3-dimensional boundary surface of constant energy that separates unfilled electron orbitals from filled orbitals at absolute zero.[2] Because, as discussed previously, the cyclotron radius of a given electron orbital depends on the electron's momentum, the effective mass will influence the shape of the Fermi surface of the material. Further, the Fermi surface depends on electron occupation and so it is related to carrier density. Therefore, because the period of SdH oscillations is determined by the Fermi surface, the oscillations will depend on carrier density and effective mass.

It was predicted that Bi nanowires which underwent the SM-SC transition would have decreased hole density due to the lowering of the band overlap energy.[6,10] This carrier density could be directly

extracted by calculating the period of SdH oscillations. The periods of the SdH oscillations of the 80, 200, and 270 nm diameter nanowire arrays were consistent with those expected to occur during the approach to the SM-SC transition.[15] The carrier density was calculated using the oscillation period and plotted in Figure 12. A substantial decrease in hole density indicates that as wire diameter decreased confinement effects caused the 200 nm and 80 nm wires to approach insulating states (with the 80 nm wires resembling semiconductors).

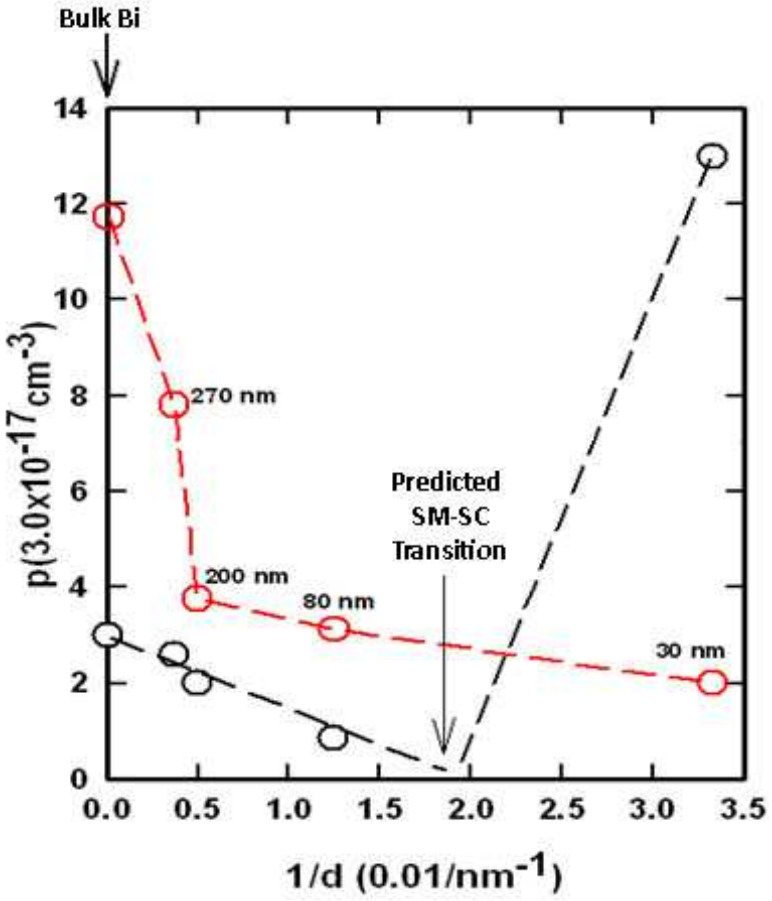

Figure 12: Hole carrier density *p* is plotted vs. inverse nanowire diameter. The predicted carrier density is plotted in red and experimental measurements in black. The expected SM-SC transition diameter is marked.[6,15]

It was predicted that the 30 nm diameter nanowires would have the lowest carrier density due to the SM-SC transition. However, the array displayed a short SdH period which was consistent with a

large carrier density ($3x10^{18}$ cm^{-3}), demonstrating an *increased* density.[6,15] The effective mass of the carriers was calculated using the temperature dependence of the SdH oscillation amplitude for the 30 nm wires. The estimated effective mass was 0.3 m_e compared to the bulk effective mass which is 0.065 m_e.[6] One possible explanation for the increased number and mass of the carriers was the dominance of surface states. As described in the **Background** chapter of this thesis, nanowires might have a surface "sheath" layer of electrons with higher effective mass. These states could be formed due to spin-orbit interaction that occurs in the presence of the surface electric field.[15] As nanowire diameter is decreased these surface states play an increasingly important role. The smaller the nanowire diameter is, the larger the ratio of surface area to volume will be. Consequently, the ratio of surface states to regular states will also be higher. It is reasonable to conclude that the electronic behavior of 30 nm diameter nanowires and the SM-SC transition could thus be influenced by the increased density and effective mass of charge carriers in surface states.[15]

The work by Huber *et al* provides substantial reason to believe that surface states play a role in preventing the SM-SC transition of nanowires with small diameters. However, there are several aspects of these magnetoresistance experiments which must be further examined in order to definitively explore the SM-SC transition and the existence of surface states. The most significant factor is the issue of electrical contact. In any given array as many nanowires as possible must be in electrical contact with the measurement system in order to provide accurate data. In this situation, however, a silver epoxy was used in the two-probe measurement and bulk Bi was used in the quasifour-probe measurement.[6] The silver epoxy was granular in nature which caused only a small fraction of the nanowires (approximately 10^{-5}) to be contacted. In the quasifour-probe measurement, it is likely that nearly all of the nanowires in each array were contacted.[6] The introduction of bulk Bi into the system, though, causes difficulty when trying to detect sensitive confinement phenomena.[6] In order to thoroughly

investigate the SM-SC transition and the existence of surface states, a "non-contact" experiment was required.

Magnetization Measurement

I played an integral role in conducting a series of non-contact experiments during 2006-2008 with Professor Michael Graf's research group.[8] Like the work previously mentioned, we conducted these experiments to measure oscillatory phenomena in order to obtain information about confinement effects. In this case, the measurement of interest was of dHvA oscillations of the material's magnetization rather than SdH oscillations.

To explore these types of magneto-oscillations we used a silicon cantilever magnetometer. The cantilever measurements were performed by first mounting a nanowire array on a flexible cantilever arm so that the axis of the nanowire array (trigonal) was oriented parallel to the surface normal of the cantilever. Then we utilized a superconducting magnet to sweep an applied magnetic field from 0 to 9 T in a ^{3}He refrigerator. As the sample became magnetized the cantilever would deflect; this deflection could be measured by observing the change in capacitance between a capacitor plate mounted on the underside of the cantilever arm and a capacitor plate on the base of the device.[8] By measuring the deflection we could calculate the degree to which the sample was magnetized.

For several measurements the cantilever was aligned so that the nanowire array axis was oriented at an angle of 13° or 81° with the field. This position is referred to as "torque mode." Because of the shape anisotropy of the wires the magnetization was directed along the nanowire axis and so the applied magnetic field caused the nanowires to line up as much as possible with the field axis (like a compass needle pointing North). This alignment behavior created an induced torque response in the

cantilever. Small displacements of the cantilever arm were assumed and so the nanowire array magnetization per volume was proportional to the fractional change of the capacitance in field H divided by magnetic field where V_{Bi} was the calculated volume of Bi for a given nanowire array.[8]

$$M\ \alpha\ \frac{C(H)-C(0)}{C(0)HV_{Bi}} \equiv \frac{\Delta C(H)}{C_0 HV_{Bi}}\ 8$$

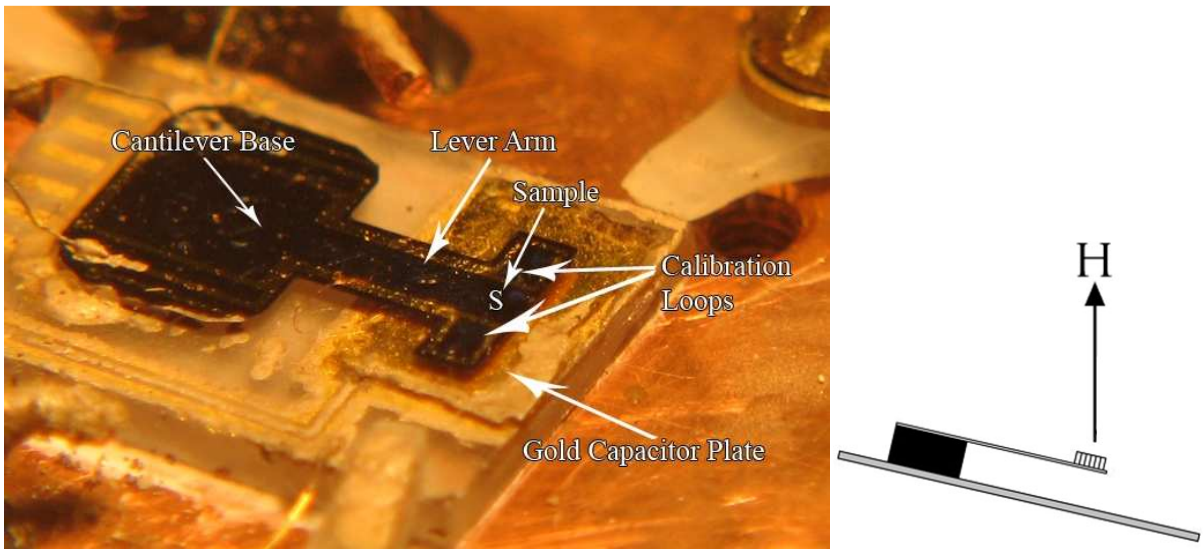

Figure 13: (Left) Photograph of the cantilever magnetometer with various components labeled. The cross of the "T" of the flexible lever arm has a capacitor plate on its underside which is suspended slightly above the gold capacitor plate. (Right) Schematic displaying the cantilever in torque mode in which the nanowire axis is oriented away from the applied field axis, H, by a certain known angle.

Arrays of 36 ± 3, 60 ± 14, and 270 ± 40 nm diameter nanowires were measured. The statistical error in nanowire diameter was calculated using SEM images.[8] Using the SEM software it was possible to make measurements of the nanowires being studied. A sample of individual nanowire diameters was measured using this software. By analyzing the deviation between the measurements for nanowires in a given nanowire array it was possible to calculate the diameter variability. These SEM images were also used to estimate the volume fractions of the Bi in the PAAO templates. The images demonstrated Bi volume fractions of 0.34 ± 0.12, 0.12 ± 0.06, and 0.37 ± 0.12 for the 36, 60, and 270 nm nanowire arrays

respectively.[8] The samples masses and associated volume calculations are displayed in the following table:

Sample	Sample Mass(g)	Mass Bi (g)	Mass Template (g)	Volume Bi (m^3)	Volume Template (m^3)
36 nm NWA	9.00E-04	5.67E-04	3.33E-04	5.80E-11	1.13E-10
60 nm NWA	2.82E-03	9.33E-04	1.89E-03	9.54E-11	6.39E-10
270 nm NWA	7.20E-4	4.75E-4	6.76E-04	4.86E-11	8.28E-11

To obtain a baseline magnetization measurement to which the Bi nanowire array measurements could be compared, measurements of empty PAAO templates were performed. This data was subtracted from the data collected from the nanowire arrays in order to assure that the magnetic response of the PAAO templates was not mistaken for the actual response of the nanowire arrays. The temperature ranges over which the nanowire arrays were measured are displayed in Figures 14 and 15. The arrays were all measured from 0 to 9 T.[8]

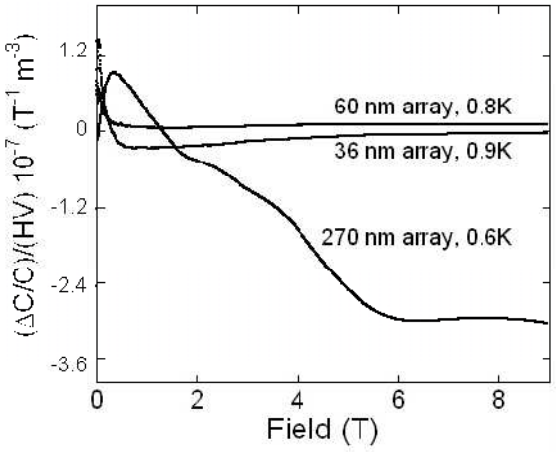

Figure 14: Magnetization per volume data for various nanowire diameters oriented at an angle of 13° to the applied magnetic field.[8]

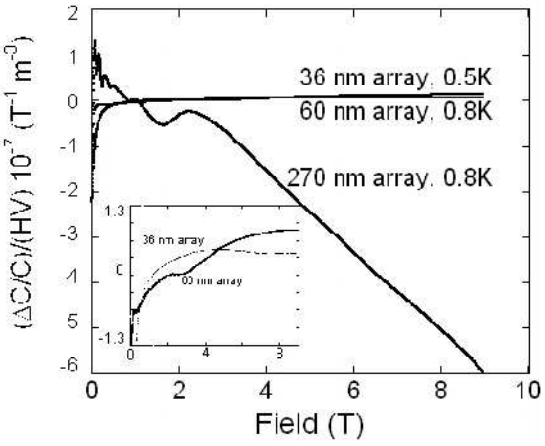

Figure 15: Magnetization per volume data for various nanowire diameters oriented at an angle of 81° to the field.[8]

One of the principal goals of this experiment was to determine whether the SM-SC transition was occurring or whether it would appear that electrons in small diameter nanowires were occupying surface states and dominating the behavior of the material. For Bi the SM-SC transition should occur when the nanowire diameter is reduced below the electron cyclotron orbit (~55 nm).[6] At this size the material's energy band gap is increased and no charge carriers are left in partially filled Landau levels. Therefore the highest level is always fully occupied, the Fermi level will no longer shift, and the material's magnetization will no longer oscillate in an applied magnetic field.[8]

Upon inspection of Figures 14 and 15 it is readily apparent that for arrays with nanowire diameters near or below the predicted SM-SC transition diameter of 55 nm the magnetization is dramatically lower than the array with 270 nm diameter nanowires. Figure 14 depicts the magnetic response for all three diameters of nanowire arrays when the cantilever is oriented at an angle of 13° with respect to the applied magnetic field axis and Figure 15 depicts the magnetic response for the three samples when cantilever is oriented at an angle of 81° with respect to the field axis.

It would be incorrect to conclude that the small signal displayed by the 36 and 60 nm diameter nanowire arrays in Figures 14 and 15 was due to a reduced amount of Bi in the arrays. While the individual 36 and 60 nm diameter nanowires obviously had smaller volumes than the 270 nm diameter nanowires, the 60 nm diameter nanowire array actually had a greater Bi mass because the array itself was larger. This important fact discounted the explanation that the small signal was due to low mass and adds strength to the idea that confinement effects were occurring.

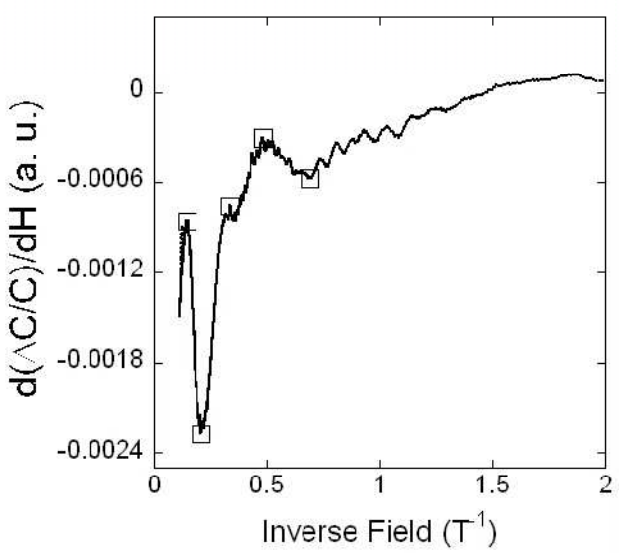

Figure 16: Derivative of magnetization with inverse field for 270 nm diameter nanowires at an orientation of 13° to the magnetic field axis. Squares indicate indexed maxima and minima.[8]

To explore the magnetization oscillations of the 270 nm diameter nanowire array, we took the derivatives of the magnetization (taken from the 13° cantilever orientation) and plotted them vs. inverse field. This plot is displayed in Figure 16. Two different oscillatory phenomena were observed. The first were small amplitude "fast" oscillations which had small periods. When the empty PAAO templates were measured these same types of fast oscillations were evident.[8] Therefore it was concluded that the oscillations were not intrinsic to the Bi. The second type of oscillations were large amplitude "slow" oscillations with large periods. These slow oscillations were attributed to the dHvA effect.[8] The period of the dHvA oscillations was calculated by indexing the inverse field locations of the maxima and minima from Figure 16 and plotting them on an integer scale. Because of the periodic nature of the oscillations the resulting plot was linear with period equal to the slope of the line. The 2 T^{-1} peak did not follow the periodic sequence and therefore was not accounted for in the calculation. It was not likely associated with the dHvA effect.[8]

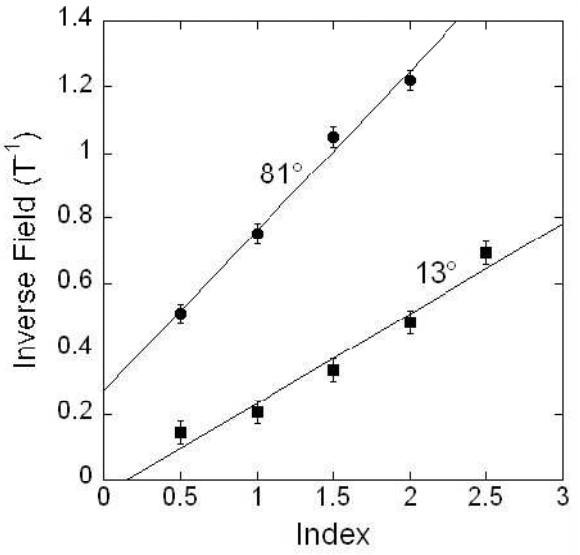

Figure 17: Indexed maxima and minima for the oscillations exhibited by the 270 nm diameter nanowire array. The slope of the lines can be calculated to obtain the period of the dHvA oscillations.[8]

The period of the dHvA oscillations in the 270 nm diameter nanowire array measured by the 13° cantilever orientation was determined to be 0.27 ± 0.03 T^{-1}. The indexed plot is shown in Figure 17. The measurements taken by the cantilever oriented at 81° with respect to the applied field displayed similar results. The dHvA period of the 270 nm diameter nanowire arrays was calculated to be 0.49 ± 0.04 T^{-1}. A full oscillation appeared to occur in the magnetization of the 36 and 60 nm diameter nanowire arrays but it was difficult to determine whether this behavior corresponded to the dHvA effect.[8]

When the trigonal axis of the nanowires was aligned at an angle of 13° with respect to the magnetic field, sources have shown that the dHvA periods for electrons should be between 0.1 T^{-1} and 0.25 T^{-1} and the period for holes should be closer to 0.16 T^{-1}.[18,19] The 0.27 T^{-1} period we measured identified that electrons were the carriers responsible for the oscillations found in the 13° cantilever orientation. The measurement of the 81° cantilever alignment agreed with these results. At an 81° angle the electron periods should be between 0.09 T^{-1} to 0.7 T^{-1} while the hole period should be 0.055 T^{-1}. The

observed period was 0.49 T^{-1} which was clearly closer to the expected periods of electrons. These results agreed with previous dHvA measurements performed using Bi microwires.[20]

It is interesting to note that in Figures 14 and 15 the 270 nm diameter nanowire array seems to experience a paramagnetic response, indicated by the positive values that occur approximately between 0 to 1 T. Bulk Bi is a diamagnetic material and so any paramagnetic response is intriguing. Arrays of 50 μm diameter microwires exhibited diamagnetic behavior with magnetization which was roughly linear with field.[20] The paramagnetic behavior in the Bi nanowire arrays was suggestive of the "Chambers peak."[8] The Chambers peak is a phenomenon observed in the magnetic field dependence of electrical resistance and occurs because of a mobility change as the cyclotron orbit of carriers become comparable to nanowire diameter. When the orbit radius is larger than the nanowire diameter electrons moving through the material begin to collide with the boundaries of the nanowire. This effect is marked by a resistivity increase because the collisions cause the electrons to move less efficiently through the material. The crossover field value at which this phenomenon occurs is given by

$$B_c = hk_F/\pi ed$$

with k_F being the carrier Fermi wave vector and d being the nanowire diameter.[21] In Bi nanowires the crossover field value B_c is approximately 1 T for 270 nm diameter nanowires and approximately 0.4 T for 60 nm diameter nanowires.[8] The lower crossover field value for 60 nm diameter nanowires is related to the SM-SC transition because the carrier concentration for these nanowires is smaller than in the bulk and so consequently k_F is smaller. Heremans *et al* studied similar k_F effects.[22] The paramagnetic behavior was not evident in the response of the 36 nm diameter nanowire arrays and further investigation is warranted on additional arrays with nanowire diameters between 60 and 500 nm.

The results of this series of experiments seemed to contradict the findings of the magnetoresistance measurements. While the measured SdH periods indicated that 30 nm diameter

nanowire arrays did not appear to undergo the SM-SC transition and instead exhibited increased carrier density, the cantilever magnetization measurements suggested that the weak signal from the 36 and 60 nm diameter nanowire arrays was due to the SM-SC transition and the consequent reduction of carrier density. The findings of our magnetization measurements indicated that the effects in the Bi nanowires was not due to electrons in surface states dominating the properties of the material. These measurements did not suffer from the electrical problems of the magnetoresistance experiment because cantilever magnetometry is a non-contact procedure. However, the anomalous paramagnetic behavior measured by the cantilever must be investigated. Until systematic investigation can concretely identify the phenomenon as the Chambers peak the possibility that it is an artifact of the measurement device cannot be ruled out. Another experiment was necessary to either confirm or deny the presence of surface states in Bi nanowires.

Heat Capacity Measurement

A third series of experiments was conceived to continue the investigation of the Bi nanowire arrays. While the previous two experiments sought to measure oscillatory effects in the conductivity and magnetization of the nanowire arrays, this experiment was unique in that it was designed to measure heat capacity, a thermal property. Like the magnetization experiment it was not necessary to make electrical contact with the nanowires in the array. To make thermal measurements a calorimeter platform with a heater and thermometer was required to introduce heat to the sample and measure how the sample responded. However, because of the small mass of the Bi nanowire arrays it was necessary to construct a calorimeter platform that had components with very low heat capacity values.

Components of Heat Capacity

The heat capacity of a material describes how the material responds to heat. Specifically, the heat capacity of a substance is defined as the amount of heat needed to increase the temperature of that substance by one degree Kelvin.[23] The heat capacity is comprised of factors due to the material's nuclear, electronic, and phononic properties. The heat capacity, C, is given by:

$$C=BT^{-2}+\gamma T+AT^{3}$$

where T is temperature and B, γ, and A are constants that relate to the nuclear, electronic, and phononic contributions to heat capacity, respectively.

By analyzing the electronic contribution to the material's heat capacity it is possible to gain information about carrier density and effective mass which could provide insight into the possible existence of surface states. As mentioned in the **Magnetoresistance Measurement** chapter, charge carriers in surface states have higher effective mass and increased number density. The γ constant, called the Sommerfeld parameter,[2] scales proportionally to the product of charge density and effective mass:[24]

$$\gamma \alpha nm^{*}$$

If charge carriers in surface states heavily influence small diameter nanowires as hypothesized by Huber *et al,* the Sommerfeld parameter should be enhanced from its value for bulk Bi; if the material undergoes the SM-SC transition and the carrier density goes to zero, the electronic contribution should be negligible.

It was important to discern at what temperature each component of the heat capacity of Bi is significant. By determining the temperature range in which the electronic contribution to heat capacity is dominant it becomes possible to make measurements to probe the existence of surface states.

Because of slow spin relaxation the nuclear contribution is not believed to contribute significantly to the heat capacity at low temperatures. This is thought to be the case because of the "slow spin-lattice relaxation" of the nuclei. This slow relaxation means that the nuclei are effectively thermally decoupled from the Bi lattice structure and so, at low temperatures, heat is not effectively exchanged.[25,26,27] Thus the nuclear contribution to heat capacity should not interfere with the measurement of the electronic contribution over any relatively low temperature range.

As temperature decreases toward 0 K the phonon contribution to the heat capacity of Bi will decrease proportionally to T^3, which is much faster than the electron contribution which decreases linearly. As can be seen in Figure 18 the phonon contribution to the heat capacity should be smaller than the bulk electron contribution to heat capacity at low temperatures, assuming for the case of argument that the "normal" Bi carrier density is unchanged by confinement. However, the phonon contribution may be enhanced when confined to the nanoscale. Because the nanowires are one dimensional structures rather than three dimensional, phonons may propagate preferentially in the growth direction of the nanowires (trigonal, [001]). The velocity of phonons in this direction is slightly lower than the velocity of phonons in the bulk material. The velocity of phonons in a bulk material is calculated by averaging the velocity of phonon propagation in all directions. Because the phonon velocity is slower, the Debye temperature (a property derived from the Debye model that describes a solid as a system of coupled oscillators) will be smaller and the phonon heat capacity component will be about two times larger.[2,4] The following calculations demonstrate the amount of expected enhancement.

$$Phonon\ velocity\ in\ bulk\ Bi\text{: } v_{bulk} = 1790\ {}^{m}/_{s}\ ^{28}$$

$$Phonon\ velocity\ (longitudinal, transverse, average) in\ [001]\ direction\ at\ 1.6K\text{:}$$

$$v_{LA} = 2.02x10^{5}\ {}^{cm}/_{s}, v_{TA} = 1.13x10^{5}\ {}^{cm}/_{s},\ \bar{v}[001] = 1.43x10^{5}\ {}^{cm}/_{s} = 1436.7\ {}^{m}/_{s}\ ^{29}$$

The Debye temperature θ_D is calculated using phonon velocity *v,* Planck's constant *ħ*, Boltzmann's constant k_B, the number of atoms in the specimen *N*, and volume *V*.[2]

$$\theta_D = \frac{\hbar v}{k_B}\left(\frac{6\pi^2 N}{V}\right)^{1/3}$$

$$\theta_{D,bulk} = \left(\frac{\hbar}{k_B}\left(\frac{6\pi^2 N}{V}\right)^{1/3}\right)(1790\,{}^{m}/_{s}) = 119K$$

$$\theta_{D,[001]} = \left(\frac{\hbar}{k_B}\left(\frac{6\pi^2 N}{V}\right)^{1/3}\right)(1435.7\,{}^{m}/_{s}) = 94.85K$$

The constant A which defines the phonon contribution to the total heat capacity of the material is described by the following relation, in which n_A Avogadro's number.[2]

$$A = \frac{12000\pi^4}{5} k_B n_A \left(\frac{1}{\theta_D}\right)^3$$

$$A_{[001]} = \frac{12000\pi^4}{5} k_B n_A \left(\frac{1}{94.85K}\right)^3 = 0.002277\,{}^{J}/_{mol * K^3}$$

$$A_{bulk} = 0.001154\,{}^{J}/_{mol * K^3}$$

Figure 18 shows that the enhanced phonon contribution is lower than the electronic contribution in bulk Bi at extremely low temperatures.

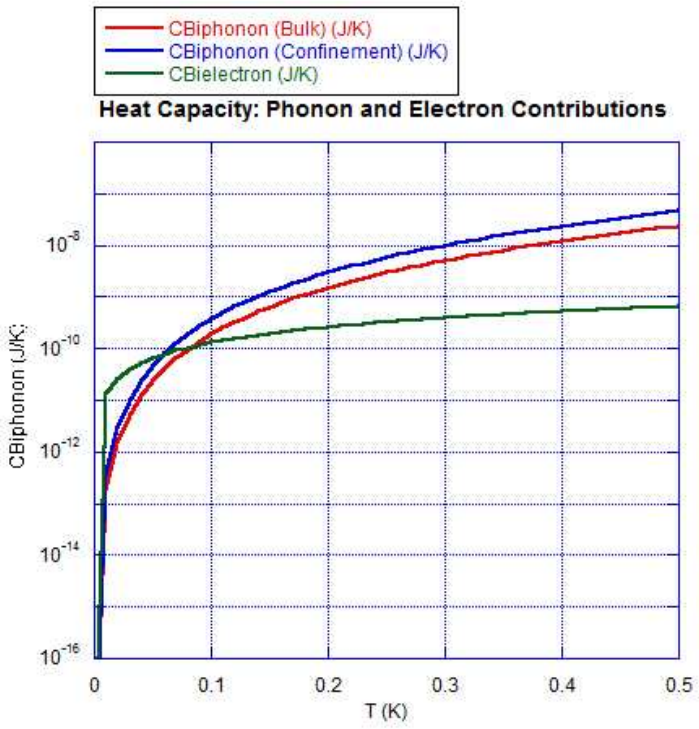

Figure 18: The phonon, enhanced phonon, and electron contributions are displayed.

Calorimeter Design Estimates

Since the electronic component of the heat capacity of the Bi nanowire arrays was expected to be small it was necessary to design a calorimeter platform which itself had an even lower heat capacity and would therefore not obscure the measurement. To minimize the heat capacity of the various "addenda" on the platform I designed a heater, thermometer, and contacts which were all metal or metal-alloy thin films. A sapphire disk was selected to serve as the platform on which to attach the Bi nanowire arrays and conduct the calorimetry experiments. The platform would have a resistor-heater to introduce heat to the system and a thermometer to measure how the nanowire arrays responded to the heat input.

A quantitative calculation of the heat capacity of the Bi in the nanowire arrays was therefore vital when designing the calorimeter. For the purpose of the following calculations the Bi heat capacity

for the nanowires was assumed to be the same as for bulk Bi. The heat capacity for the wires may be different if carriers in surface states dominate the properties of small diameter nanowires, but this bulk approximation was useful for estimation purposes.

At temperatures below the Fermi Temperature and the Debye temperature the heat capacity of bulk Bi can be represented by the following equation:

$$C_{Bi} = \gamma T + AT^3 \; {}^{J}/_{mol*K} = 0.000008T + 0.001154T^3 \; {}^{J}/_{mol*K}$$

γ and A were found using experimental data for bulk Bi provided in Charles Kittel's *Introduction to Solid State Physics*.[2]

Heat capacity is an extensive property and so this equation must be multiplied by the amount of Bi present, expressed in the unit "moles" (1 mol = 6.02 x 10^{23} atoms). The masses of the Bi in the 36, 60, and 270 nm diameter nanowire arrays were the same as those listed in the **Magnetization Measurement** chapter with one addition. The two stacks of 7 nanowire arrays that I prepared at Howard University had a combined mass of 0.52 milligrams (mg).

$$moles(36nm\ array) = (9.0x10^{-4}g)\left(\frac{1\ mol}{208.9804\ g}\right) = 2.7x10^{-6}mol$$

$$moles(60nm\ array) = (2.82x10^{-3}g)\left(\frac{1\ mol}{208.9804\ g}\right) = 4.5x10^{-6}mol$$

$$moles(270nm\ array) = (1.99x10^{-3}g)\left(\frac{1\ mol}{208.9804\ g}\right) = 6.29x10^{-6}mol$$

$$moles(270nm\ array\ stack\ of\ 7) = (5.20x10^{-2}g)\left(\frac{1\ mol}{208.9804\ g}\right) = 1.64x10^{-4}mol$$

The PAAO templates used to create the nanowire arrays also contributed to the heat capacity of the total system. The following heat capacity equation was extrapolated from data presented in a previous paper.[30]

$$C_{Temp} = 0.0002575T^{2.6306} \; {}^{J}/_{mol*K}$$

The number of moles of template in each sample was calculated using volume fraction estimates.

$$moles(36nm\ Temp.) = (3.32x10^{-4}g)\left(\frac{1\ mol}{101.9613\ g}\right) = 3.26x10^{-6}mol$$

$$moles(60nm\ Temp.) = (1.89x10^{-3}g)\left(\frac{1\ mol}{101.9613\ g}\right) = 1.85x10^{-5}mol$$

$$moles(270nm\ Temp.) = (6.76x10^{-4}g)\left(\frac{1\ mol}{101.9613\ g}\right) = 6.63x10^{-6}mol$$

$$moles(270nm\ Temp.\ stack\ of\ 7) = (1.77x10^{-2}g)\left(\frac{1\ mol}{101.9613\ g}\right) = 1.73x10^{-4}mol$$

A sapphire disk was used to construct the calorimeter platform. The temperature dependent heat capacity of sapphire was extrapolated using previous experimental data.[31]

$$C_{Saph} = (1x10^{-11})T^{3.025}\ {}^{J}/_{mol*K}$$

The mass of a sapphire disk was measured to calculate the number of moles of sapphire in a typical disk.

$$moles(Saph.Disk) = (4.69x10^{-2}g)\left(\frac{1\ mol}{101.9613\ g}\right) = 4.60x10^{-4}mol$$

Gold (Au) wire was first considered for use on the calorimeter but was ultimately rejected because of its high heat capacity value. The following calculation was performed using constants found in Kittel's textbook.[2] The wires that would have been used had diameters of 25 μm and were 1 cm in length.

$$C_{Au} = 0.000729T + 0.000433T^3\ {}^{J}/_{mol*K}$$

$$moles(Au\ wire) = \pi\left(\frac{25\mu m}{2}\right)^2(0.01m)(19.3x10^6\frac{g}{m^3})\left(\frac{1\ mol}{196.97\ g}\right) = 4.81x10^{-7}mol$$

Aluminum (Al) wire has a relatively high heat capacity value in the "normal regime" but below T_c=1.163K the material becomes superconducting and has a much lower heat capacity value.[32] The heat

capacity in the normal temperature regime was found using experimental constants listed in Kittel's text and the heat capacity relation in the superconducting regime was drawn from previous research.[2,32]

$$C_{Al\,Wires\,(Normal)} = 0.00135T + 2.48x10^{-5}T^3\ {}^{J}/_{mol*K}$$

$$C_{Al\,Wires\,(Superconducting)} = 7.1T_c\exp\left(\frac{-1.34T_c}{T}\right)(1.350x10^{-3})\ {}^{J}/_{mol*K}$$

$$moles(Al\ wire) = \pi\left(\frac{25\mu m}{2}\right)^2(0.01m)(2.7x10^6\,\frac{g}{m^3})\left(\frac{1\ mol}{26.98\ g}\right) = 4.91x10^{-7}mol$$

For this experiment a thin film Au-Germanium (Ge) alloy thermometer was created. The thermometer had extremely small mass and a consequently low heat capacity value. The thermometer was 0.25 x 1 mm^2 in area and 51 nm thick. The alloy was approximately 18% Au and 82% Ge. C_θ is the heat capacity of the thermometer.

$$C_{Au} = 0.000729T + 0.000433T^3\ {}^{J}/_{mol*K}$$

$$C_{Ge} = 0.000372T^3\ {}^{J}/_{mol*K}$$

$$C_\theta = [0.18(C_{Au}) + 0.82(C_{Ge})][0.18(moles\ Au) + 0.82(moles\ Ge)]$$

$$moles\ Au = (2.5x10^{-7}m^2)(51x10^{-9}m)(19.3x10^6\,\frac{g}{m^3})\left(\frac{1\ mol}{196.97\ g}\right) = 1.25x10^{-9}mol$$

$$moles\ Ge = (2.5x10^{-7}m^2)(51x10^{-9}m)(5.32x10^6\,\frac{g}{m^3})\left(\frac{1\ mol}{72.64\ g}\right) = 9.34x10^{-10}mol$$

A thin film Nichrome (NiCr) resistor was made to serve as a way to introduce to the sample. Several calculations were performed in order to determine the ideal dimensions of the thin film so that the resistor would exhibit suitable resistance at low temperatures while still possessing a low heat capacity. The best dimensions were determined to be: length 3 mm, width 0.5 mm, and thickness 20 nm. The resistivity of NiCr as a function of temperature is known.[33]

$$\rho_{NiCr} = (1x10^{-6}\Omega m) + \left(4x10^{-12}\,\frac{\Omega m}{K}\right)T \quad \text{(For 0.1K<T<1K} \quad \rho\sim10^{-6}\ \Omega m\text{)}$$

$$R_{NiCr} = \rho\frac{L}{A} = \rho\frac{0.003m}{1x10^{-11}m^2} \quad \text{(For 0.1K<T<1K} \quad R\sim300\ \Omega\text{)}$$

The NiCr alloy is 80% Nickel (Ni) and 20% Chromium (Cr). C_h in the following equation indicates the heat capacity of the heater.

$$C_{Cr} = 1.40T + 0.0078T^3 \ {}^{mJ}/_{mol}$$

$$C_{Ni} = 7.02T + 0.0213T^3 \ {}^{mJ}/_{mol}$$

$$C_h = [0.8(C_{Ni}) + 0.2(C_{Cr})][moles\ NiCr]$$

$$moles(NiCr\ Heat.) = (1x10^{-11}m^2)(0.003m)(8.4x10^6 \frac{g}{m^3})\left(\frac{1\ mol}{57.35\ g}\right) = 4.39x10^{-9}mol$$

In order to make electronic connection to the thermometer and heater four Au pads were made that were 0.5 x 0.5 mm^2 in area and 150 nm thick.

$$C_{AuPad} = 0.000729T + 0.000433T^3 \ {}^{J}/_{mol}$$

$$moles(4\ Au\ Pads) = (4)(6.25x10^{-8}m^2)(150x10^{-9}m)(19.3x10^6 \frac{g}{m^3})\left(\frac{1\ mol}{196.97\ g}\right) = 3.67x10^{-9}mol$$

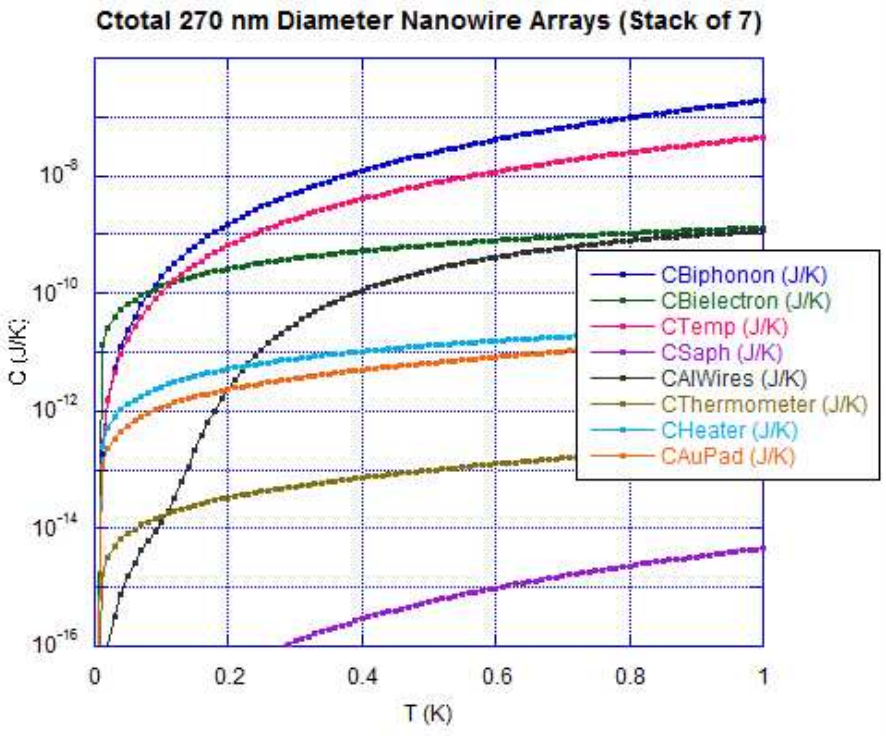

Figure 19: The heat capacity contributions of the various calorimeter and sample components are displayed on a logarithmic plot.

Estimated Magnitude of Confinement Effects

To estimate whether confinement effects would be observable, I compared the heat capacity of nanowires if no confinement effects were to occur with the heat capacity of nanowires if confinement effects did occur. The ratio was calculated for a 270 nm diameter nanowire array with 2 mg mass at 0.2 K. Such a sample would consist of 1.3 mg Bi and 0.68 mg PAAO template. The ratio *R* would be represented by:

$$R = \frac{(C_{el,NWA} + C_{ph} + C_{temp})}{(C_{el,bulk} + C_{ph} + C_{temp})}$$

with $C_{el,NWA}$ the electron contribution to the heat capacity of the nanowire arrays, $C_{el,bulk}$ the electron contribution to the heat capacity of the bulk material, C_{ph} the phonon contribution to the heat capacity, and C_{temp} the template contribution. Three possibilities are likely. They are:

1. No confinement effects will occur. In this situation $C_{el,NWA} = C_{el,bulk}$ and R = 1.
2. The SM-SC transition occurs due to confinement and the nanowires in the arrays become semiconducting. If this effect happens $C_{el,NWA} = 0$ and R < 1.
3. The number density and effective mass of the carriers is larger than would be expected due to the dominance of carriers existing in surface states as quoted by Huber *et al*.[6] In this case, because γ α nm*, $C_{el,NWA} = 25C_{el,bulk}$.

The following calculations demonstrate the value of R for the array mentioned above at 0.2 K.

$$C_{temp} = (0.2575T^{2.6})(mols\ temp.) = 2.59x10^{-11}\ {}^{J}/_{K}$$

$$C_{ph} = (1.154T^{3})(mols\ Bi) = 5.82x10^{-11}\ {}^{J}/_{K}$$

$$C_{el,bulk} = (0.008T)(mols\ Bi) = 1.01x10^{-11}\ {}^{J}/_{K}$$

$$C_{el,NWA} = 25(0.008T)(mols\ Bi) = 2.52x10^{-10}\ {}^{J}/_{K}$$

R = 3.6

So, if the measured electronic component of the heat capacity was enhanced by a factor of 3.6, it could be concluded that carriers were existing in surface states similar to those discussed by Huber *et al*.

Calorimeter Construction

As evidenced by the calculations in the ***Calorimeter Design Estimates*** section, it was necessary to utilize a variety of experimental methods in order to precisely create calorimeter platform components with ultra low heat capacity contributions. One particular technique I used to fabricate components with low masses and low heat capacities was photolithography. Photolithography enables the design of microscopic patterns on a material which can be used as the first step in creating small scale devices. The process works by first depositing a thin layer of a "photoresist" material on a substrate and then using ultraviolet (UV) light to selectively etch areas of the photoresist.[14] After certain patterns are created on a substrate using photolithography, metal is deposited using thermal evaporation.

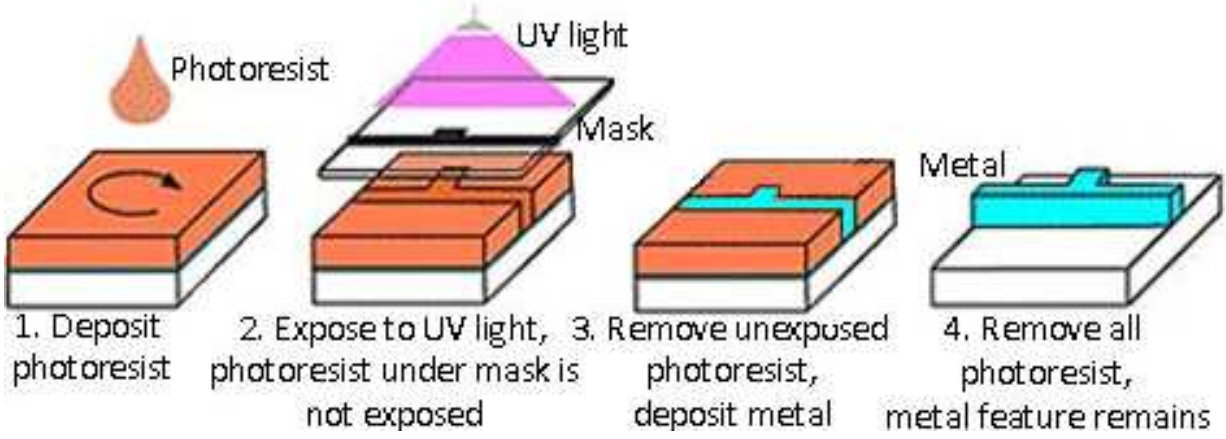

Figure 20: A diagram illustrating the photolithography process.

In order to control which areas of the photoresist are exposed to the UV light I prepared a special mask was using the software program L-Edit.

Figure 21: Mask patterns used for photolithography. From left to right: the thermometer contacts, the thermometer, the heater, and four Au contacts. The small rectangles present on the left and top of each pattern are for alignment purposes.

I created the previous mask design to be applied to construct the calorimeter platform as displayed in Figures 22 and 23.

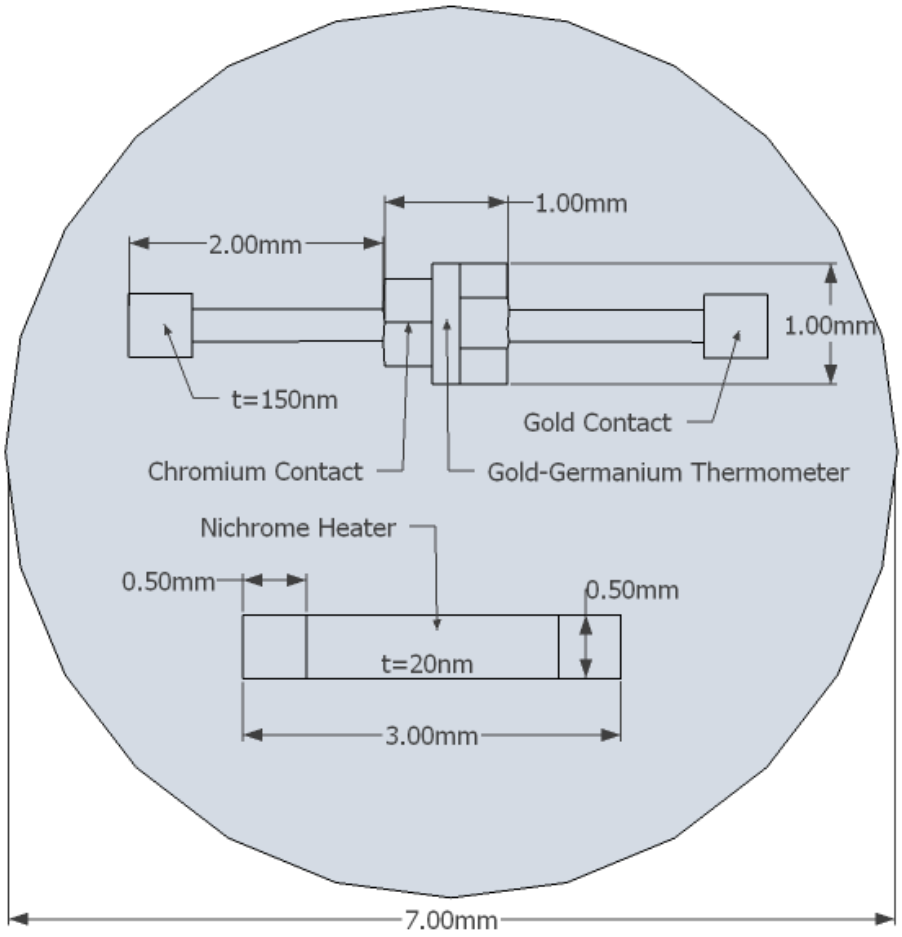

Figure 22: A blueprint used to construct the calorimeter plate.

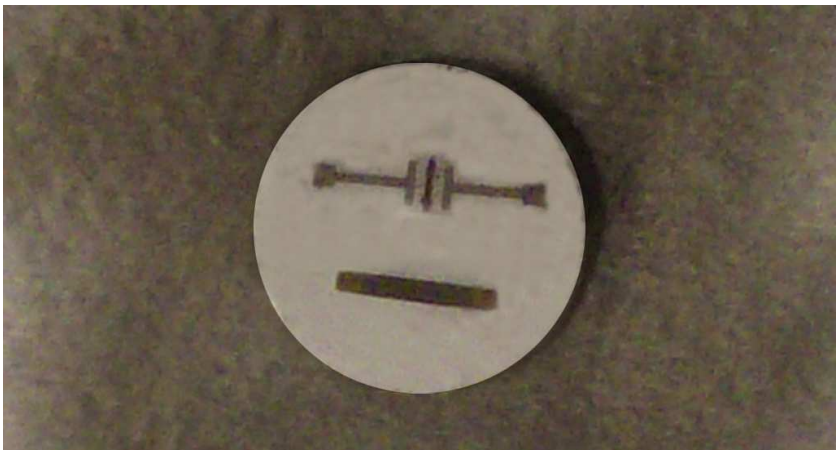

Figure 23: Photograph of the calorimeter plate.

Experimental Techniques

Ac-temperature (ac-T) calorimetry is a powerful technique that was selected to measure the electronic contribution to the heat capacity of the various Bi nanowire arrays.[34] Typically ac-T calorimetry is used to measure small changes in the heat capacity of a material due to phenomena such as phase transitions, but it is also useful for materials which equilibrate quickly after a heat pulse is introduced. For ac-T calorimetry the amplitude of the temperature variation of a sample is measured when an oscillating voltage of a certain period is supplied to a heater.[34] The relaxation time constants (the time it takes the system to equilibrate after heat is introduced) for the various parts of the system must be known to determine the correct frequency for the oscillating voltage. The time period of the oscillations must be longer than the internal equilibration time of the calorimeter and sample, but much shorter than the characteristic time it takes for heat to flow out of the system. If these conditions are met, then the amplitude of the temperature variation is inversely proportional to the total heat capacity of the system.[34]

The ac-T calorimetry technique was developed by Sullivan and Seidel who published a paper describing their method in 1968.[34] In order to collect thermal data an ac-heating current with frequency $\frac{1}{2}\omega$ was used. The current was supplied to a heater made from an electric resistor which was connected to the sample being studied. In their case the sample was a small amount (82 mg) of Beryllium (Be).[35]

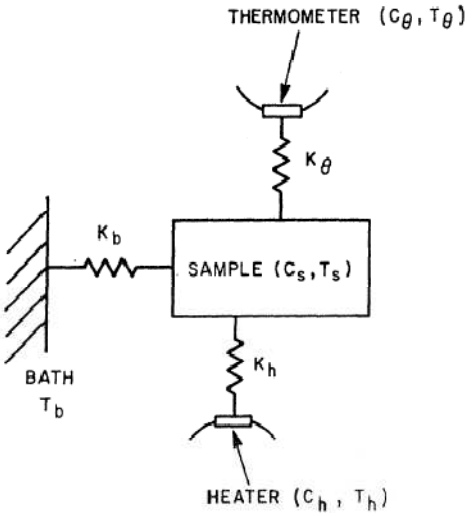

Figure 24: Diagram of a sample coupled to a thermometer, heater, and bath by thermal conductances K_θ, K_h, and K_b respectively.

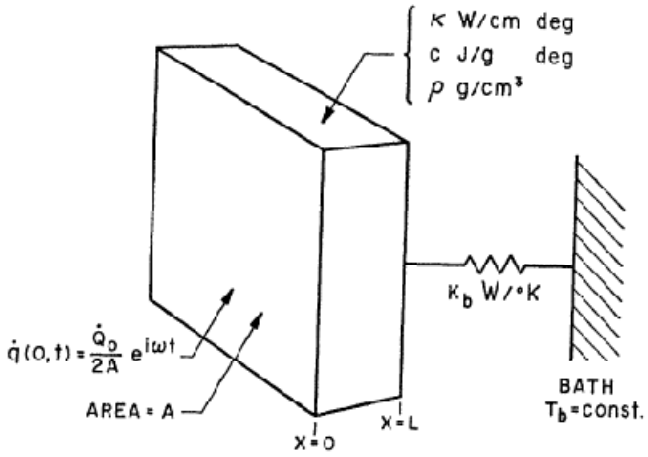

Figure 25: A sample of thickness L is thermally connected to a bath and has sinusoidal heat input.

Under the conditions displayed in the above diagrams, the temperature response of the material could be described by

$$T_{ac} = \frac{Power}{2\omega C}(1 + \frac{1}{\omega^2\tau_1^2} + \omega^2\tau_2^2 + constant)^{-1/2}$$

where T_{ac} is the temperature measured by the thermometer, *Power* is the input power (in watts), τ_1 is the sample-to-bath relaxation time, τ_2 is the response time of the sample, heater, and thermometer to the heat input, and C is the total heat capacity. τ_1 is described by

$$\tau_1 = \frac{C}{K_b}$$

where K_b is the thermal conductance between the sample and the bath. τ_2 is described by

$$\tau_2^2 = \tau_\theta^2 + \tau_h^2 + \tau_{int}^2\,, \qquad \tau_{\theta=}\frac{C_\theta}{K_\theta}, \qquad \tau_{h=}\frac{C_h}{K_h}, \qquad \tau_{int=}\frac{L^2}{(90)^{1/2}\,n} = \frac{\rho c_s L^2}{(90)^{1/2}K_s}$$

with $\tau_\theta, \tau_h, \tau_{int}$, as the system's thermometer, heater, and internal time constant, respectively. *L* is the thickness of the sample, *n* is the thermal diffusivity, *ρ* is the density, c_s is the specific heat, and K_s is the thermal conductance of the sample.[34]

By keeping τ_2 much less than $\frac{1}{\omega}$ and keeping τ_1 much greater than $\frac{1}{\omega}$ the heat capacity of the sample can be described by

$$C = \frac{Power}{2\omega T_{ac}}(1 + const)^{-1/2}$$

with the *const* term given by $2K_b/3K_s$. This equation is quite powerful.[35] Heat capacity can thus be calculated using only a few easily measured parameters.[34]

The following calculations and figures display the values of τ_1 and τ_2 for the previously mentioned stack of 7 arrays of 270 nm diameter nanowires. For the purposes of the calculations, the Bi nanowires were assumed to behave as if they were in the bulk state. The conductivity of the Al wires is given when they are in their superconducting state (T < 1.16K).[36]

$$\tau_1 = \frac{C_{Bi,Phonon} + C_{Bi,Electron} + C_{saph} + C_{temp} + C_\theta + C_h + C_{wires} + C_{contacts}}{K_{wires}}$$

$$K_{wires} = (0.0036exp(4.0664T))\left(\frac{\pi\left(25x10^{-6}/2\right)^2}{0.01}\right)$$

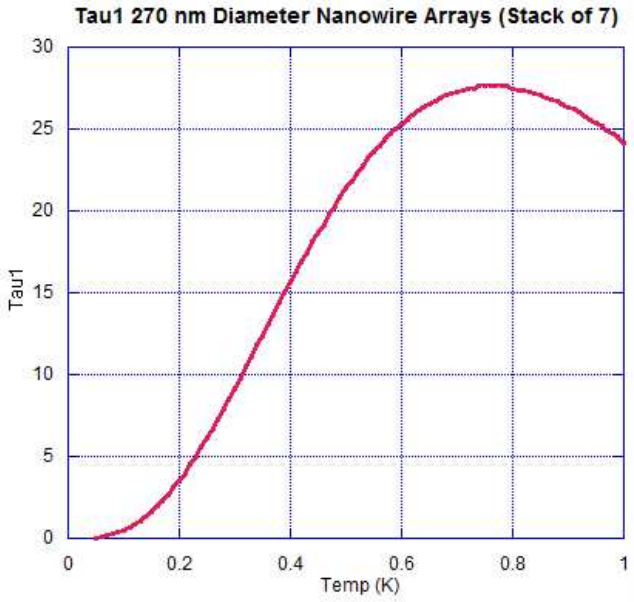

Figure 26: The low temperature time constant τ_1 for a certain nanowire array sample.

The heat capacities of the various materials have been described in the ***Calorimeter Construction*** section of this work and the thermal conductivity values of Au, Ge, and Bi were obtained from various sources.[37,38,39] The thermal conductivity of NiCr can be calculated using its known electrical conductivity (the reciprocal of the resistivity calculated in the ***Calorimeter Construction*** section).[39]

$$\tau_{\theta=}\frac{C_\theta}{K_\theta}=\frac{[0.18(0.000729T+0.000433T^3)+0.82(0.000372T^3)][9.91x10^{-10}]}{[0.18(31T)+0.82(0.1359\exp(4.3397T))][\frac{2.5x10^{-7}}{51x10^{-9}}]}$$

$$\tau_{h=}\frac{C_h}{K_h}=\frac{[0.2(0.0014T+0.0000078T^3)+0.8(0.00702T+0.0000213T^3)][4.39x10^{-9}]}{\left(\frac{2.20T}{1x10^{-6}+4x10^{-12}T}+6.0\right)(\frac{1.5x10^{-6}}{20x10^{-9}})}$$

$$\tau_{int=}=\frac{\rho c_s L^2}{(90)^{1/2}K_s}=\frac{(9780)(0.000008T+0.001154T^3)(0.00097)^2}{\sqrt{90}(0.0179T)(\frac{2.14x10^{-7}}{0.000107})}$$

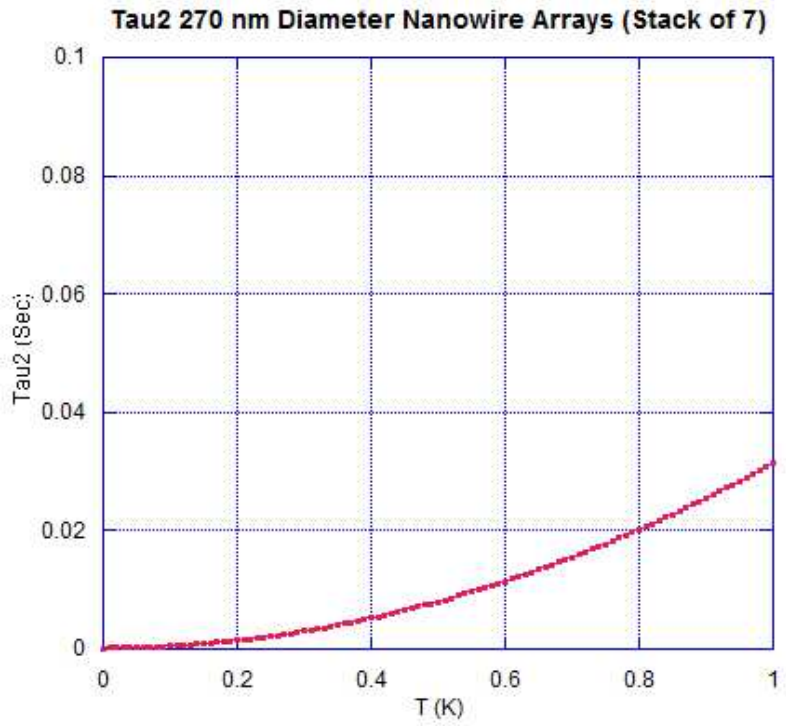

Figure 27: The low temperature time constant τ_2 for a certain nanowire array sample

Clearly, for the selected sample τ_2 will be much less than τ_1 and thus suitable for use in ac-T calorimetry.

Dilution Refrigerator

It is necessary to perform the heat capacity measurements at low temperatures and so the experiments must be conducted in a dilution refrigerator. The dilution refrigerator functions by a phase separation of various isotopes of Helium (He). As can be seen in Figure 28, if the temperature of a ^{3}He-^{4}He mixture which has more than 6% ^{3}He is lowered, the mixture will separate into two distinct phases.[40]

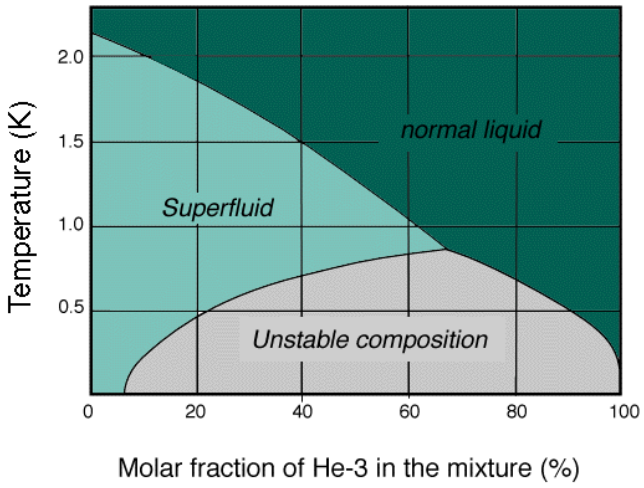

Figure 28: Phase diagram of liquid He

At very low temperatures, one of these phases will be nearly pure ^{3}He and the other will be mostly ^{4}He with a 6% ^{3}He impurity.[40] If the concentrated phase of ^{3}He and the dilute phase are brought into contact, and if the liquid-vapor interface on the dilute phase side is kept at 0.7 K, most of the vapor will be ^{3}He. A pump can be used to remove the vapor and destroy the equilibrium between the two phases. In a dilution fridge the liquid-vapor interface exists in the “mixing chamber” displayed in Figures 29 and 30.

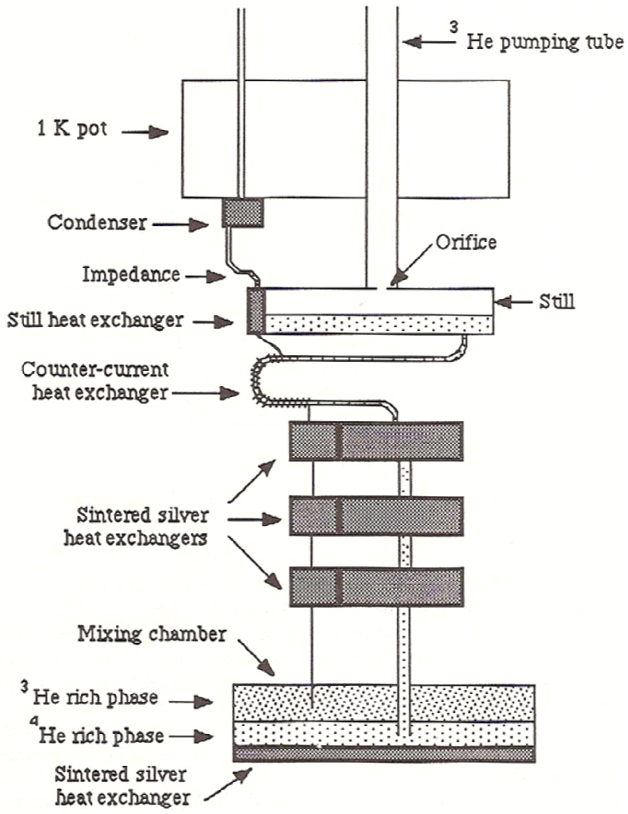

Figure 29: Schematic of a typical dilution fridge[40]

To restore equilibrium ^{3}He atoms will "evaporate" across the phase boundary from the concentrated ^{3}He rich region into the dilute region.[40] The process requires thermal energy, which can be supplied by an experimental sample which will be attached to the "heat exchanger" below the mixing chamber. This removal of thermal energy is how the sample is cooled.[40] Temperatures as low as 2.3 mK have been reached using dilution refrigerators.[43] Our dilution refrigerator can achieve a minimum temperature of approximately 20 mK. It has been shown in the ***Heat Capacity Components*** and ***Calorimeter Design Estimates*** sections that it is necessary to reach these low temperatures in order to ensure the measurement of the electron contribution to the material's heat capacity. At higher temperatures the phonon contribution to the heat capacity and the heat capacity of the various calorimeter components may mask the electronic contribution.

Figure 30: Photograph of the dilution refrigerator that would be used for this experiment. The calorimeter in which the sample is housed is depicted at the bottom of the image and is connected to the heat exchanger. The mixing chamber is the silver cylinder connected to the heat exchanger.

Applications

One of the reasons it is so important to understand the nature of the confined charge carriers in Bi is that Bi nanowire arrays have possible thermoelectric applications. Thermoelectrics is a technological field with great potential. By using thermoelectric materials it is possible to create two highly useful devices: the first type uses electric current to cool and the second utilizes a temperature gradient to generate electricity.

Typical metals heat up as current is conducted through them. This heat is essentially wasted energy and is often detrimental to the system. Certain thermoelectric materials behave quite differently

than traditional conductors, however. By using these materials it is actually possible to construct devices that cool (by absorbing heat from an external object) as current passes through them. This phenomenon is referred to as the "Peltier effect."[42]

Both n and p-type semiconducting materials are used when manufacturing thermoelectric cooling devices. The positive terminal of a voltage source is connected to an electrode which is attached to piece of n-type material. The other side of the n-type material is connected to another electrode which is connected both to the surface to be cooled and to a piece of p-type material. The other end of the p-type material is connected to another electrode which is then connected to the negative terminal of the voltage source. This system is a complete closed circuit. Current flows from the positive terminal of the voltage source through one electrode and through the n-type material. It then flows across the electrode which is connected to the cooling surface and then through the p-type material. Current returns through the last electrode to the negative terminal of the voltage source.

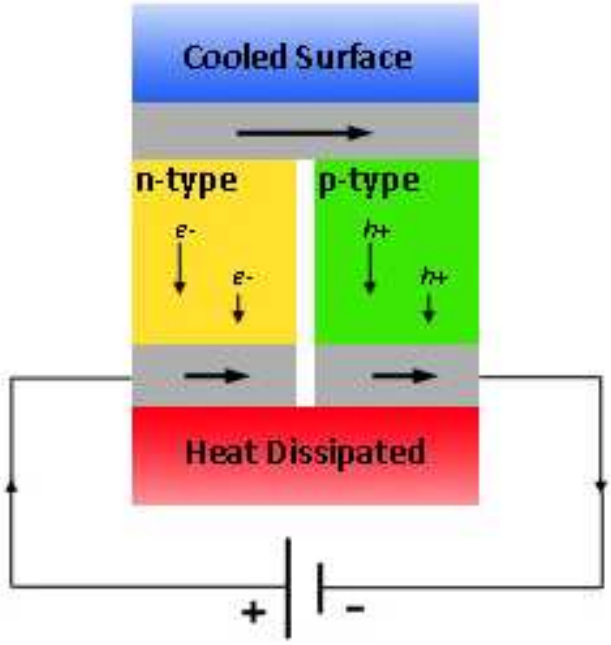

Figure 31: The arrows in this diagram illustrate the path current would take. The specimen is attached to the "cooled surface" and heat is dissipated via a heat sink. Electrons and holes are represented by e^- and h^+ respectively.

The movement of electrons and holes is responsible for the cooling that occurs on the intended surface. As current flows the few electrons in the p-type material move into the electrode and then into the n-type material. Upon entering the n-type material they are excited to a higher energy level. This process requires the absorption of thermal energy. The necessary heat is drawn from the attached specimen, thus cooling it.[42]

The type of thermoelectric cooling device previously described is a "solid state" component because it does not involve the transfer of liquids or gases and does not have any mechanical moving parts. Modern refrigerators use tetrafluoroethane which alternates between liquid and gas phase as it is pressurized and depressurized.[44] This process involves various motors, pumps, and valves. These components wear down over time and if one of them breaks the system may not function correctly. Solid state devices have no moving parts that will wear down or break. For this reason thermoelectric coolers are longer lasting and more resilient than modern refrigerators. Thermoelectric coolers are currently used on deep space probes to regulate the temperatures of various components. Because engineers cannot easily make repairs on these probes they must use devices that are very mechanically tough.[45] Solid state devices meet this need.

A second kind of thermoelectric device can convert heat into electricity using the "Seebeck effect."[46] Like the thermoelectric cooling effect, this effect requires both n and p-type semiconducting materials. Unlike the cooling device, though, no voltage source is required to drive the flow of electrons and holes. Instead, a temperature gradient causes the carriers to move. Both electrons and holes will migrate from high temperatures to low. This movement causes an electric current to manifest in the device.[47]

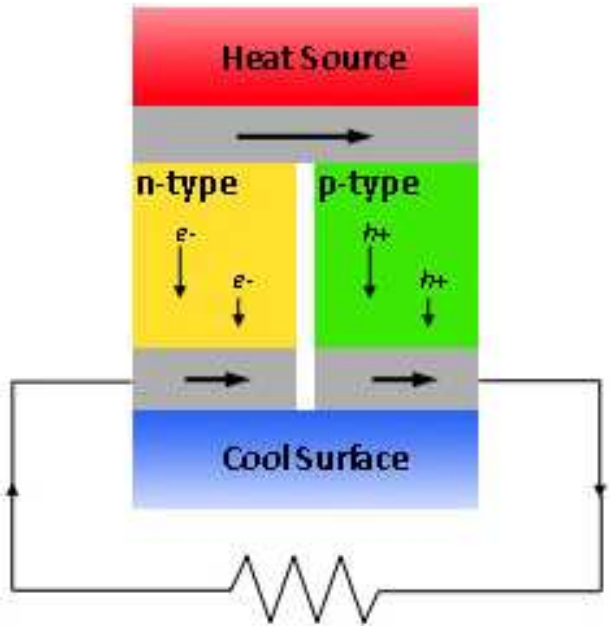

Figure 32: The electrons and holes flow from the "heat source" to the "cool side." Their movement produces a current indicated by the direction of the arrows. In the diagram the current is flowing through a resistor represented by the zigzag line.

The potential applications for this type of current-generation are vast. Heat is produced by nearly all forms of technology, including cars, computers, and even light bulbs. For the most part, this heat is a completely wasted form of energy. Utilizing this thermoelectric effect is a highly appealing way to take advantage of that energy. It would be possible to put a thermoelectric device in a car, for example, in such a way that the engine would serve as the heat source which drives the movement of charge carriers. This device may be superior to the contemporary method of using an alternator to charge the car's battery. Like thermoelectric coolers, thermoelectric current-generating devices have no moving parts and therefore are more durable and easier to maintain than mechanical systems. Thermoelectric devices could also be used in unison with photovoltaic technology to increase the energy generated by solar cells. As solar cells collect light from the sun, the panels heat up. Thermoelectric devices could capture this heat to supplement the power generation of the cells.

Thermoelectric devices have vast potential but are currently inefficient and prohibitively expensive to produce.[45] The magnitude of the currents and temperature gradients necessary to foster the desired thermoelectric effects are not economically feasible. In order to increase the efficiency of thermoelectric devices the materials used must allow current to pass through relatively unimpeded while at the same time not allowing heat from the heat sink to travel back to the cooled surface. If the hot and cold surfaces equilibrate the temperature gradients will be eliminated and the devices will not function.

Bi possesses the unique combination of high electrical conductivity and low thermal conductivity. In its bulk state Bi has a high "thermoelectric figure of merit."[48] A material's thermoelectric figure of merit is defined as

$$ZT = \frac{S^2 \sigma T}{\kappa}$$

where *S* is the thermoelectric power (Seebeck coefficient), σ is electrical conductivity, and κ is thermal conductivity.[49] A high figure of merit (greater than 1) indicates an efficient thermoelectric material.[46]

Bulk Bi has one of the highest figures of merit for any material at temperatures below 100 K.[48] It has been hypothesized that confinement effects may enhance Bi's already favorable thermoelectric properties. The increased density of carrier states that may occur in Bi nanowires would help to increase the material's figure of merit.[49] As discussed in the **Magnetoresistance Measurements** chapter, certain diameter nanowires may have increased carrier density due to the dominance of carriers in surface states. If these types of theorized confinement effects do occur, Bi nanowires will be quite useful if fabricated in arrays. Arrays of nanowires offer high sample mass while still retaining favorable quantum properties.

Conclusion

Bi is an intriguing material to study when it is confined to the nanoscale. Bulk Bi is a semimetal with a small number of low effective mass charge carriers.[6] These properties cause the material to be particularly sensitive to confinement effects such as the SM-SC transition. Further, for small diameter nanowires high effective mass charge carriers in surface states may dominate the behavior of the material.

Magnetoresistance measurements were performed on 270, 200, 80, and 30 nm diameter nanowire arrays. All exhibited periodic SdH oscillations. For the 270, 200, and 80 nm diameter nanowires low carrier densities indicated that as wire diameter decreased confinement effects caused nanowires to approach semiconducting or insulating states. The 30 nm diameter nanowires, however, displayed oscillations indicative of increased effective mass and density of charge carriers, possibly due to the dominance of carriers in surface states.[6,15]

To continue investigating the confinement effects the magnetization of arrays of 36, 60, and 270 nm diameter nanowires were measured. It was clear that the 36 and 60 nm diameter nanowire arrays, which had diameters near or below the predicted SM-SC transition diameter of 55 nm, had reduced magnetic responses when compared to the 270 nm diameter nanowires. The oscillation periods of the 270 nm diameter nanowires identified electrons as the carriers responsible for the dHvA oscillations.[8,18,19] The magnetization measurements seemed to contradict the conclusions drawn from the magnetoresistance measurements. The lack of dHvA oscillations for the 36 and 60 nm diameter nanowire arrays suggested that they experienced the SM-SC transition and that the nanowire response was not influenced by electrons in surface states.

Measurements of the electronic contribution to heat capacity were proposed to reconcile the results of the previous experiments. If the electronic contribution to the heat capacity was enhanced

from its predicted bulk value it could be concluded that high effective mass electrons in surface states were strongly affecting the material's behavior. I performed detailed calculations and determined that it would be feasible to use ac-T calorimetry to measure this possible enhancement. At low temperatures (~T < 1 K) reached using a dilution refrigerator the nuclear and phononic contributions to the heat capacity of the material would not mask the electronic contribution.

Because samples with large Bi mass were required I traveled to Howard University to learn the pressure injection technique and create my own nanowire array samples. During my time at Boston College I designed a sapphire calorimeter plate with ultra-low heat capacity components. This endeavor required many theoretical calculations to decide the ideal geometries for the various components and the correct materials to use for each. Using photolithography and thermal deposition of metal I constructed a thin-film thermometer, heater, and contacts. These components, as well as the (superconducting) wires used, all had heat capacity values significantly lower than the expected value of the electronic contribution.

This thesis project was an incredible educational experience. I gained a deep understanding of the physics that govern the heat capacity of a material as well as knowledge about the complicated confinement effects that may occur in Bi nanowires. I received direct instruction about a useful sample fabrication technique and was given the opportunity to create my own nanowire arrays. Further, I learned numerous experimental methods when designing and creating my calorimeter platform. This thesis project has drawn to a close but I have confidence that another student will receive the torch that I am passing and continue to strive to understand the fundamental nature of these interesting structures.

Works Cited

1. Griffiths, David J. Introduction to Quantum Mechanics. Second ed. Upper Saddle River, NJ: Pearson Prentice Hall, 2005.

2. Kittel, Charles. Introduction to Solid State Physics. New York: John Wiley & Sons, Incorporated, 2004.

3. "Intrinsic Semiconductor." Hyperphysics. Georgia State University. <http://hyperphysics.phy-astr.gsu.edu/hbase/solids/intrin.html>.

4. Keer, H. V. Principles of the Solid State. New York: J. Wiley & Sons, 1993.

5. Casiday, Rachel, and Regina Frey. "Bonds, Bands, and Doping: How Do LEDs Work?" Washington University in St. Louis, Department of Chemistry. <http://www.chemistry.wustl.edu/~courses/genchem/Tutorials/LED/bands_06.htm>.

6. T. E. Huber, A. Nikolaeva, D. Gitsu, L. Konopko, C. A. Foss, Jr., and M. J. Graf, Applied Physics Letters **84**, 1326 (2004).

7. J. C. G. de Sande and J. M. Guerra, Phys. Rev. B **45** (1992).

8. R. C. Johnson, J. R. Riley, T. E. Huber, and M. J. Graf, J. Phys.: Conf. Ser. **150**, 022030 (2009).

9. "Infinite Potential Well." Wikimedia Commons. <http://commons.wikimedia.org/wiki/File:Infinite_potential_well.svg>.

10. Y. Lin, X. Sun, and M.S. Dresselhaus, Phys. Rev. B **62**, 4610 (2000).

11. "Anopore Inorganic Membranes (Anodisc)." Whatman - Leadership in Separations Technology for the Life Sciences. <http://www.whatman.com/PRODAnoporeInorganicMembranes.aspx>.

12. Universidad Complutense de Madrid :: UCM. <http://www.ucm.es/info/mclab/magneto-optics/nanowires.jpg>.

13. T. E. Huber, M. J. Graf, C. A. Foss, Jr., and P. Constant, Journal of Materials Research **15**, 1816 (2000).

14. Hornyak, Gabor L., Joydeep Dutta, Harry F. Tibbals, and Anil K. Rao. Introduction to Nanoscience. Boca Raton: CRC P, 2008.

15. Huber, Tito E. "Quantum Confinement and Surface State Effects in the Thermopower of Bismuth Nanowires." March Meeting of the American Physical Society. Baltimore, Maryland. Mar. 2006.

16. SJSU Department of Physics and Astronomy. <http://www.physics.sjsu.edu/becker/physics51/images/28_13A_Orbit_in_B_field.jpg>. (Copyright Addison Wesley Longman Inc.)

17. "Shubnikov-de Haas effect." Словари и энциклопедии на Академике. <http://dic.academic.ru/dic.nsf/enwiki/3024014>.

18. R. D. Brown III, Phys. Rev. B **61**, 6631 (2000).

19. G. E. Smith, G. A. Baraf, and J. M. Rowell, Phys. Rev. **135**, A1118 (1964).

20. M. J. Graf, C. P. Opeil, and T. E. Huber, Journal of Low Temperature Physics **134**, 1055 (2004).

21. T. E. Huber, K. Celestine, and M. J. Graf, Phys. Rev. B **67**, 245317 (2003).

22. J. Heremans, C. M. Thrush, Y. M. Lin, S. Cronin, Z. Zhang, M. S. Dresselhaus, and J. F. Mansfield, Phys. Rev. B **61**, 4850 (2000).

23. Ebbing, Darrell D., and Steven D. Gammon. General chemistry. Eighth ed. New York: Houghton Mifflin, 2005.

24. Ashcroft, Neil W., and N. David Mermin. Solid State Physics. New York: Holt, Rinehart and Winston, 1976.

25. M. M. Krishna and B. N. Srivastava, Solid State Communications **12**, (1973).

26. H. K. Collan, M. Krusius, and G. R. Pickett, Phys. Rev. B **1**, 7 (1970).

27. H. K. Collan, M. Krusius, and G. R Pickett, Phys. Rev. **23,** 1 (1969).

28. WebElements Periodic Table of the Elements. <http://webelements.com/>.

29. Madelung, O., U. Rössler, and M. Schulz, eds. Landolt-Börnstein - Group III Condensed Matter. Vol. 41C. Springer, 1998.

30. G. T. Furukawa, T. B. Douglas, R. E. McCoskey, and D. C. Ginnings, Journal of Research of the National Bureau of Standards **57**, 2 (1956).

31. E. C. Kerr, H. L. Johnston, N. C. Hallet, JACS **72**, 10 (1950).

32. N. E. Phillips, Phys. Rev. **114**, 3 (1959).

33. Meier, Mike. Electrical Resistivity as a Function of Temperature. Department of Chemical Engineering and Materials Science, University of California Davis, 2004.

34. P. F. Sullivan, G. Seidel, Phys. Rev. **173**, 3 (1968).

35. G. R. Stewart, Review of Scientific Instruments **54**, (1983).

36. C. B. Satterthwaite, Phys. Rev. **125**, 3 (1962).

37. G. K. White, Proc. Phys. Soc. **A559**, (1953).

38. A. Kumar and M. M. Joshi, Phys. Rev. B **4**, 4643 (1971).

39. Billings, Bruce. American Institute of Physics Handbook. New York: McGraw Hill, 1963.

40. Richardson, Robert C., and Eric N. Smith, eds. Experimental Techniques in Condensed Matter Physics at Low Temperatures. Reading, Ma: Addison-Wesley, 1998.

41. UCB: 3He-4He Dilution Explanation. UC Berkeley. <http://cdms.berkeley.edu/UCB/75fridge/inxsrc/dilution/phd.gif>.

42. Godfrey, Sara. "How the Thermoelectric Works." Electronics Cooling. <http://www.electronics-cooling.com/articles/1996/sep/sep96_04.php>.

43. D. I. Bradley, M. R. Follows, I. E. Miller, R. Oswald, and M. Ward, Cryogenics **34**, 549 (1994).

44. "How Does a Refrigerator Work?" How Things Work. <http://www.energyquest.ca.gov/how_it_works/refrigerator.html>.

45. Minkel, J R. "Novel Semiconductor Device Heats and Cools on a Dime." Scientific American. <http://www.sciam.com/article.cfm?id=novel-semiconductor-devic>.

46. "Introduction to Thermoelectrics." Thermoelectrics.com. <http://www.thermoelectrics.com/introduction.htm>.

47. THERMOELECTRICS AND THE 12 MOST FREQUENTLY ASKED QUESTIONS ABOUT THERMOELECTRIC COOLING. Tellurex Corporation. <http://www.tellurex.com/12most.html#top>.

48. Goldsmid, H. J. Electronic Refrigeration. Second Ed. London: Pion, 2005.

49. L. D. Hicks and M. S. Dresselhaus, Phys. Rev. B **47**, 12727 (1993).

50. S. M. Bhagat and D. D. Manchon Jr., Phys. Rev. **164**, 3 (1967).